Coupling of TRPV6 and TMEM16A in epithelial principal cells of the rat epididymis

Da Yuan Gao,[1]* Bao Li Zhang,[1]* Matthew C.T. Leung,[2] Simon C.L. Au,[2] Patrick Y.D. Wong,[2] and Winnie W.C. Shum[1]

[1]School of Life Science and Technology, ShanghaiTech University, Shanghai 201210, China
[2]School of Biomedical Sciences, The Chinese University of Hong Kong, Hong Kong Special Administrative Region, China

The epididymis establishes a congenial environment for sperm maturation and protection. Its fluid is acidic, and the calcium concentration is low and declines along the length of the epididymal tubule. However, our knowledge of ionic currents and mechanisms of calcium homeostasis in rat epididymal epithelial cells remains enigmatic. In this study, to better understand calcium regulation in the epididymis, we use the patch-clamp method to record from single rat cauda epididymal principal cells. We detect a constitutively active Ca^{2+} current with characteristics that match the epithelial calcium channel TRPV6. Electrophysiological and pharmacological data also reveal a constitutively active calcium-activated chloride conductance (CaCC). Removal of extracellular calcium attenuates not only the TRPV6-like conductance, but also the CaCC. Lanthanide block is time dependent such that the TRPV6-like component is inhibited first, followed by the CaCC. The putative CaCC blocker niflumic acid partially inhibits whole-cell currents, whereas La^{3+} almost abolishes whole-cell currents in principal cells. Membrane potential measurements reveal an interplay between La^{3+}-sensitive ion channels and those that are sensitive to the specific TMEM16A inhibitor tannic acid. In vivo perfusion of the cauda epididymal tubule shows a substantial rate of Ca^{2+} reabsorption from the luminal side, which is dose-dependently suppressed by ruthenium red, a putative blocker of epithelial Ca^{2+} channels and CaCC. Finally, we discover messenger RNA for both TRPV6 and TMEM16A in the rat epididymis and show that their proteins colocalize in the apical membrane of principal cells. Collectively, these data provide evidence for a coupling mechanism between TRPV6 and TMEM16A in principal cells that may play an important role in the regulation of calcium homeostasis in the epididymis.

INTRODUCTION

The epididymis in the male reproductive tract is lined with a layer of epithelial cells, which creates a unique environment for the immature spermatozoa from the testis to undergo the most essential posttesticular morphological and functional changes, thus conferring them with the potential for motility and capacity to undergo acrosome reaction (Turner, 1995; Hermo and Robaire, 2002; Cooper, 2007; Dacheux and Dacheux, 2014; Robaire and Hinton, 2015). By the time the spermatozoa reach the cauda epididymis, they are mature, yet they are held and protected in a dormant state during storage. Sperm function thus directly depends upon the specialized luminal fluid established by epididymal epithelial cells (Carr and Acott, 1984; Hong et al., 1984; Turner, 2002; Dacheux and Dacheux, 2014). Identified in these cells are the various transporters, ion channels, and pumps that work in a concerted manner to create the luminal microenvironment for the most needed physiological changes to take place in the spermatozoa. One of the features in the epididymal fluid, as demonstrated by micropuncture studies in rats, is that it is slightly acidic, with low levels of calcium and chloride ions, and these ionic gradients decline prominently along the epididymal tubule (Levine and Marsh, 1971; Turner, 2002). The physiological implication of this special calcium homeostasis in the epididymal microenvironment is not fully clear, but it is believed that low calcium levels are essential to prevent immature activation of sperm in the dormant stage in the head region of the epididymis (Hong et al., 1985; Schuh et al., 2004).

The calcium ion (Ca^{2+}) is known to serve as a first messenger in extracellular space of organisms and a key second messenger in live cells through the regulation of countless biochemical processes, and therefore, their levels have to be tightly controlled. The luminal Ca^{2+} concentration decreases from ~1.9 mM in the testicular fluid to 1.3 mM in the proximal epididymal regions, and then to as low as 0.25 mM in the posterior cauda regions (Levine and Marsh, 1971; Jenkins et al., 1980; Turner, 2002; Weissgerber et al., 2011). Taking into consideration that >90% of the testicular fluid is removed when it reaches the epididymis (Wong and Yeung, 1978; Cooper, 2007), this means that >90% of the Ca^{2+} in the luminal fluid is absorbed through the epididymal epithelial

---

The Rockefeller University Press $30.00
J. Gen. Physiol. 2016 Vol. 148 No. 2   161–182
www.jgp.org/cgi/doi/10.1085/jgp.201611626

161

cells back to the blood circulation, which implies that an efficient calcium absorption machinery is functioning in the epididymis. However, the mechanisms of Ca^{2+} homeostatic regulation in this organ are not yet fully understood. It is known that gene deletion or mutation of the epithelial calcium channel TRPV6 in mice has been shown to cause severe impairment of male fertility accompanied by abnormal accumulation of Ca^{2+} in the epididymis, highlighting the key roles of Ca^{2+} homeostatic regulation and TRPV6 for Ca^{2+} absorption in this organ for sperm health (Weissgerber et al., 2011, 2012). However, it has been reported that detection of TRPV6 current in native epithelial cells is difficult, regardless of the phenotype of *TRPV6*-deficient mice (Hoenderop et al., 2005; Weissgerber et al., 2011; Stoerger and Flockerzi, 2014), and the mechanisms by which TRPV6 carries out its functions remain unclear.

The present study aimed to determine what ionic currents are present in the primary epithelial cells isolated from the rat epididymal cells and to characterize their physiological properties using a whole-cell patch-clamp technique and pharmacological tools. This would allow us to obtain information on their physiological role and the underlying regulatory mechanism. To this end, our study demonstrates a constitutively active TRPV6-like conductance in epithelial cells of rat cauda epididymis, and unexpectedly, we also measured calcium-activated chloride conductance (CaCC) coupled with TRPV6 channel activity. Using conventional reverse transcription (RT) PCR and immunolabeling methods, together with electrophysiological and pharmacological studies, we identified TMEM16A is the molecular candidate for the CaCC, which was detected for the first time in the apical membrane of principal cells of the epididymis where TRPV6 is also predominantly located. Immunofluorescent labeling showed that TRPV6 and TMEM16A colocalized in the apical membrane of principal cells of the epididymis in a regional-dependent manner. Collectively, our study demonstrates a coupling mechanism between TRPV6 and TMEM16A in epididymal principal cells whereby TMEM16A participates as a functional partner to modulate TRPV6 activity. Their potential role in the homeostatic control of calcium levels, and possibly chloride secretion and fluid formation, in the cauda epididymal tubule is proposed and discussed.

MATERIALS AND METHODS

Experimental animals

All animal experiments were performed in accordance with the guidelines on the use of laboratory animals established by the Animal Ethics Committee of the Chinese University of Hong Kong and ShanghaiTech University. Adult male Sprague–Dawley rats weighing ~300–350 g were used, and all animals were euthanized with sodium pentobarbital anesthesia or by cervical dislocation before experiments.

Total RNA extraction and RT-PCR

To isolate total RNA from tissue samples, the rat efferent duct, kidney, and different regions of the epididymides were frozen in liquid nitrogen immediately after dissection and then homogenized using a Pro200 homogenizer (Pro Scientific Inc.) in RLT lysis buffer with the RNeasy Mini kit (QIAGEN). Total RNA was isolated according to the manufacturer's manual, and genomic DNA contamination was removed by on-column incubation with DNase I for 30 min at room temperature using the RNase-Free DNase set (QIAGEN). Isolated total RNA was stored at −80°C until being subjected to RT. Total RNA samples were reverse transcribed for 1 h at 42°C in a final volume of 50 µl with 1× RT buffer (10 mM Tris-HCl, pH 8.3, and 50 mM KCl), 5 mM $MgCl_2$, 1 mM each of dNTP, 1 U/µl RNase inhibitor, 5 µM random hexamers, 5 µM oligo(dT)$_{18}$ primer, and 2.5 U/µl MuLV RT (Applied Biosystems and Thermo Fisher Scientific). The resulting first-strand cDNA was directly used for PCR of epithelial calcium channels and calcium-activated chloride channels. Oligonucleotide primer pairs were designed to amplify a short sequence in rat TRPV5 (GenBank accession no. NM_053787.2), rat TRPV6 (NM_053686.1), and rat TMEM16A (NM_001107564). Primer sequences are as follows: TRPV6 (forward, 5′-CCTTCATGTACAGCATCACCTA-3′, and backward, 5′-CATACTCTCGCCCACATATCC-3′), TRPV5 (forward, 5′-CACCACATGCTGTGTTTACC-3′, and backward, 5′-GGCACCAACTCTGAAGATGT-3′), and TMEM16A (forward, 5′-TTCAGTTCGGCTTCGTCACCC-3′, and backward, 5′-CCAGCTTCCCGACACCTC-3′). A primer pair (forward, 5′-AGAGAGAGGCCCTCAGTTGCT-3′, and backward, 5′-TGGAATTGTGAGGGAGATGCT-3′) was included for glyceraldehyde 3-phosphate dehydrogenase, which served as the internal standard.

Reaction mixtures consisted of a 20-µl final volume containing 2 µl template, 1.25 U AmpliTag Gold DNA polymerase (Applied Biosystems and Thermo Fisher Scientific), 50 mM KCl, 10 mM Tris-HCl, pH 8.3, 2.0 mM $MgCl_2$, 1.0 mM dNTP, and 0.5 µM of forward and reverse oligonucleotide primers. The PCR mixtures were then subject to a number of amplification cycles performed in a thermal cycler with following parameters: 8 min at 95°C to activate the polymerase, followed by various cycles (28 for TRPV6, 40 for TRPV5, and 35 for TMEM16A) for 1 min at 95°C, annealing for 30 s at 60°C, extension for 1 min at 72°C, and a final extension for 10 min at 72°C. The PCR products were resolved on 2.5% agarose gel and visualized by staining with ethidium bromide or Gelstar Stain (Lonza). The amplified PCR products for epithelial calcium channel TRPV5 and TRPV6 were confirmed by sequencing. The rat kidney was used as positive control for TRPV5. Negative

controls were performed by omitting the cDNA template from the PCR amplification.

Immunocytochemistry and immunofluorescent microscopy

Immunocytochemistry was performed as previously described (Chow et al., 2004) for the detection of TRPV6 protein in rat epididymis. Paraffin sections of rat epididymis from young adult male Sprague–Dawley rats weighting between ~300 and 450 g were used. Tissues were fixed in Bouin solution overnight at 4°C. After washes, the tissues were dehydrated, embedded in paraffin, and sectioned at 4-µm thickness. Consecutive sections were heat treated to 60°C to dewax and hydrated in PBS. Antigen retrieval was performed by treatment in 10 mM citrate buffer, pH 6, for 2 min in a microwave oven. Slice sections were then treated with methanol containing 3% (vol/vol) hydrogen peroxide for 30 min to quench endogenous peroxidase activity. After rinsing with PBS, sections were incubated in blocking serum (Vectastain Elite ABS kit; Vector Laboratories) for 30 min. Excess serum was drained off, and the slice sections were incubated with primary antibodies diluted in PBS with 0.01% Triton X-100, 0.01% Tween 20, and 0.1% BSA at 4°C overnight. Sections were rinsed three times with PBS before incubation with biotinylated secondary antibody (ABC kit). After washing with PBS, the sections were incubated with Vectastain Elite ABC reagent (ABC kit) for 1 h and finally washed three times with PBS. Visualization of antigen localization was achieved by immersing sections in peroxidase substrate solution (DAB substrate kit; Vector Laboratories) until the desired stain intensity developed. Slides were rinsed with water, counterstained with Lillie–Mayer hematoxylin, dehydrated, cleared with xylene, and mounted for light microscopy examination. The images were captured by Spot-RT charge-coupled device (CCD) color camera (Diagnostic Instruments, Inc). Two primary polyclonal rabbit anti-TRPV6 antibodies targeting the C terminus (Alomone Labs) and the N terminus (ADI) were used to confirm the cellular localization of TRPV6, and they showed similar immunohistochemical reaction patterns. Negative controls were obtained by incubation with antigen-preabsorbed antibodies overnight at 4°C.

Immunofluorescent labeling using cryosections of rat epididymis was performed as described previously (Shum et al., 2011) for the detection of cellular localization TMEM16A protein. Adult rat epididymis were fixed by immersion with 4% paraformaldehyde in PBS overnight at 4°C and washed for at least three times with PBS and cryoprotected in PBS containing 30% sucrose. Tissues were then cryoprotected by embedding in Tissue-Tek OCT (Sakura), cryosectioned with a microtome (CM1950; Leica Biosystems) at 5–10-µm thickness, and stored at 4°C until use. Rabbit anti-TMEM16A antibody

was used (Abcam). For double labeling of TMEM16A and TRPV6, the TMEM16A signal was amplified using a TSA amplification kit (PerkinElmer) for both antibodies, which were of rabbit origin. Immunolabeled sections were examined using TCS-SP8 (Leica Biosystems) or A1R (Nikon) confocal microscopy. Digital images or serial stacks were imported into ImageJ software and then projected and exported as TIFF files. The TIFF images were not postprocessed, although brightness and contrast adjustment were applied to entire images using Photoshop version 9.0 software (Adobe Systems).

Isolation of epididymal cells from rat cauda epididymis

Cauda epididymal cells were isolated as previously described (Cheung et al., 2005). The lower abdomen of young adult rats (~300–350 g) was opened and the caudal part of the epididymis removed. After dissecting away the connective tissues and fat, the cauda epididymis was then finely cut with scissors and placed in sterile Hank's balanced salt solution (HBSS) containing 0.35% (wt/vol) trypsin (Type II-S, 1,800 U/mg; Sigma-Aldrich) for 30 min at 32°C with shaking. The cell suspension was then spun down, and the supernatant was discarded. The resuspended cells were incubated in HBSS containing 0.1% collagenase at 32°C with shaking for 1 h to obtain disaggregated cells. The disaggregated cells were then washed with HBSS and cultured in EMEM supplemented with 1 nM testosterone for at least 4 h or overnight as to remove fibroblasts. Epithelial cells were then harvested and reseeded onto a culture dish, kept in an incubator, and used for patch-clamp experiments on the day of isolation or the next day. Epithelial cells were viewed under an inverted microscope equipped with a differential interference contrast (DIC) optical system and identified by their distinct morphology as well as electrical properties recorded after successful whole-cell patch-clamp configuration was established on the cells.

Electrophysiological whole-cell recording of isolated epididymal cells

Isolated primary epididymal cells were harvested from the culture dish with a plastic pipette and transferred to a 1-ml chamber mounted on the stage of an inverted microscope, maintained at room temperature, and perfused at ~2 ml/min with a physiological salt solution (PSS) for at least 5 min before doing any recording. The whole-cell configuration of the patch-clamp technique was used to measure macroscopic current under voltage clamp, as described previously (Cheung et al., 2005). The resting membrane potentials were also monitored quickly by switching from voltage-clamp mode to current clamp with the current set at zero. Axopatch-200B amplifier and pClamp8 software packages were used for protocol generation and data acquisition (Axon Instruments). Patch pipettes were pulled from

borosilicate glass (Sutter Instrument) and had a resistance of 5–10 MΩ. Current data were filtered at 1–2 kHz and digitized at 2–5 kHz (steps or ramps; in 5-s intervals unless otherwise stated) or at 200 Hz (continuous holding current), respectively. Cells were routinely held at −60 mV, unless otherwise indicated. The input resistance was measured from the step change in current induced by a 10-mV hyperpolarizing step applied from holding potential of −60 mV immediately after whole-cell establishment. Cell capacitance and series resistance were also estimated from the raised transient current. Series resistance was not compensated, and no leak current was subtracted.

The standard PSS used for recording current and membrane potential consisted of 140 mM NaCl, 4.7 mM KCl, 1.2 mM $MgCl_2$, 1.2 mM NaH_2PO_4, 2.5 mM $CaCl_2$, 10 mM glucose, and 10 mM HEPES, pH 7.4, with NaOH. In nominally Ca^{2+}-free PSS, the $CaCl_2$ was omitted; in divalent-free PSS, Ca^{2+} and Mg^{2+} were replaced with Na^+. The perfusion speed was ~2 ml/min in the patch-clamp setup. The internal (pipette) solution contained 35 mM KCl, 100 mM K-gluconate, 2 mM $MgCl_2$, 3 mM Mg-ATP, 0.1 mM EGTA, and 10 mM HEPES, pH 7.2, with KOH (potassium-based 0.1 mM EGTA). In some experiments, the EGTA concentration in the pipette solution was raised from 0.1 mM to 5 mM in order to complete the intracellular Ca^{2+} chelation (potassium-based 5 mM EGTA), whereas equal molar amounts of KCl and NaCl in bathing solution were replaced with CsCl (Cs-PSS) to suppress K_{ir} currents and with NMDG-Cl (Cs-NMDG PSS) to suppress the nonspecific "leaky" cationic currents, respectively. For some experiments, intracellular K-gluconate was replaced with Cs-methanesulfonate in order to suppress the K^+ currents (caesium-based 0.1 mM EGTA or 5 mM EGTA as indicated). To further characterize the TRPV6 current, low chloride extracellular and internal solutions were used as to suppress chloride conductance, which was composed of 140 mM Na-gluconate, 4.7 mM CsCl, 1.2 mM $MgCl_2$, 1.2 mM NaH_2PO_4, 2.5 mM $CaCl_2$, 10 mM glucose, and 10 mM HEPES, pH 7.4, with NaOH (low chloride Cs-PSS). The pipette solution was set to contain 125 mM Cs-methanesulfonate, 10 mM CsCl, 1 mM $MgCl_2$, 4 mM Na_2-ATP, 10 mM BAPTA, and 10 mM HEPES, pH 7.2, with CsOH (low chloide Cs-pipette).

Fixation and immunofluorescent labeling of isolated epididymal cells

To confirm the expression of TRPV6 in epididymal principal cells after isolation, dispersed epididymal epithelial cells prepared for electrophysiological recording were plated on glass coverslips and washed briefly with PBS before fixation with methanol for 20 min. After several washes with PBS, cells were permeabilized with 0.1% Triton X-100 for 4 min and washed with PBS. Cells were blocked with 1% BSA for 30 min at room tempera-

ture before the incubation for at least 1 h with the primary antibody against TRPV6 protein at a concentration of 1:300 or 1:400 (ADI). After several washes with PBS, an FITC-conjugated donkey anti–rabbit secondary antibody (Sigma-Aldrich) was applied at 1:100 dilution concentration. Immunolabeled cells were viewed with an epifluorescence microscope, and images were captured with a CCD camera.

Membrane potential measurement using $DiBAC_4(3)$

$DiBAC4(3)$ is a voltage-sensitive fluorescent dye with excitation maxima at ~490 nm and emission maxima at 516 nm. Hyperpolarization results in extrusion of the dye and then a decrease in fluorescence (and vice versa for depolarization). Before measuring fluorescence, isolated epididymal cells were incubated in normal PSS (as used for the patch-clamp study) containing 0.5 µM dye for at least 30 min at room temperature. Cells were imaged using confocal microscopy (A1R; Nikon). Data were collected at an interval of 30 s or 1 min. Fluorescence intensity raw data were collected using Element software (Nikon), background subtracted and normalized to the mean fluorescent intensity of all cells at time zero for each set of the experiment using Excel software (Microsoft), and then further processed with Prism software for final presentation.

Intracellular calcium concentration $[Ca^{2+}]_i$ measurement

Cells were loaded with the fluorescent dye fluo3-acetoxymethyl ester (Fluo-3-AM; Molecular Probes) as described previously (Cheung et al., 2005), bathed in 2.5 mM Ca^{2+} PBS solution, and perfused at a rate of ~2 ml/min. An excitation wavelength of 488 nm was provided by a laser-scanning confocal imaging system (MRC-1000; Bio-Rad Laboratories), and fluorescence signals were collected using a 515-nm long-pass emission filter. Data analyses were performed with MetaFluor. The change in fluorescence intensity after the designed treatments was normalized with the initial intensity.

Microperfusion of rat cauda epididymis

Microperfusion of rat cauda epididymis was performed as previously described (Wong and Yeung, 1978; Shum et al., 2011). Adult male Sprague–Dawley rats weighing 350–450 g were anesthetized with sodium pentobarbitone with an intraperitoneal dose of 50 mg/kg body weight, and a few small doses were given to maintain the animals under anesthesia. Epididymides from both sides of the animal were cannulated with catheters with a tip diameter of ~200 µm and perfused simultaneously at a rate of ~2 µl/min with a perfusion solution using an infusion pump (Harvard Apparatus), displacing the spermatozoa or perfusate was collected to the 0.5-ml Eppendorf tubes through the vas deferens inserted with a polyethylene tubing with a tip diameter of ~300–400 µm.

The perfusion solution buffered with 10 mM of either HCO_3^- or HEPES was composed of 140 mM NaCl, 4.7 mM KCl, 1.2 mM $MgCl_2$, 1.2 mM NaH_2PO_4, 1.0 mM $CaCl_2$, and 10 mM glucose, pH 7.4, with NaOH. The pH was set to 7.4 with NaOH. The concentration of $CaCl_2$ was altered as indicated during the experiment. The HCO_3^--buffered solution was gassed with carbogen (95% O_2 and 5% CO_2) for at least 20 min before the experiment. After a clearance of spermatozoa from the lumen of the perfused region of epididymis and a pre-equilibration period, the perfusates were collected in Eppendorf tubes with a layer of paraffin oil on the top to prevent evaporation, and the time for each sample collection was noted and included in calculation. The time interval of the switch between solutions was ~5–10 min, which was omitted from the data points. The perfused segments of the epididymis were measured after the microperfusion experiments, and the mean length was ~18 cm, which was the value used to calculate the perfusion rate. The collected samples (usually ~60 µl) were then diluted at a 1:1 ratio with 20 mM MES buffer, pH 5.0, sealed tightly, and stored at 4°C until used for to determine the calcium concentration.

Ca²⁺ concentration determination in microperfused perfusates

The concentrations of Ca^{2+} ions in the perfusates were determined using a colorimetric method and was performed by the University Pathology Service Unit (Princess of Wales Hospital), which is affiliated with The Chinese University of Hong Kong. In brief, calcium ions were chelated by o-cresolphthalein complexone to form a purple complex calcium-o-cresolphthalein. The optical density of the purple complex was measured using a commercial kit for the calcium ion concentrations in a direct proportional manner to a standard curve using a microplate reader at 575 nm. The rate of Ca^{2+} absorption by the perfused cauda epididymis was calculated and expressed as nanomoles/squared centimeters/minutes by normalizing to the surface area, which integrated the measured length and diameter of the perfused cauda epididymis and the perfusing time for each sample collection. For each data point, at least three epididymides from different animals were included.

Data analysis

Data are presented as means ± SEM. Student's *t* test was used for the comparison between two groups, and multiple comparisons using ANOVA with Bonferroni post-hoc test was used for the comparisons for more than two groups. P-values <0.05 were accepted as significant. For electrophysiological data, whole-cell current analysis was first performed using pClamp8 software (Axon Instruments) and then exported to Excel. Figures were prepared using Prism and/or Photoshop software.

RESULTS

Regional and cellular localization of epithelial Ca²⁺ channel TRPV6 along the male excurrent duct

Conventional RT-PCR analysis was used to confirm the expression of TRPV6 mRNA in the different regions of rat epididymis and efferent duct (Fig. 1 A). However, no PCR products were detected for TRPV5 in these tissues, although they were found in the rat kidney, indicating that TRPV5 mRNA is not expressed at a detectable level in the male excurrent duct. These results were reproduced in separate RT-PCR reactions using mRNA from at least three rats. Immunohistochemical analysis using the rabbit anti–rat antibody against the N terminus of TRPV6 was employed to determine the cellular localization of TRPV6, which was found in the apical membrane of principal cells of corpus and cauda epididymides as well as in the ciliated cells of the efferent duct (Fig. 1, B–F). In the proximal initial segment, narrow cells were also positively immunolabeled. In the distal initial segment and caput epididymis, immunopositivity for TRPV6 was diffusely localized over the principal cells. In the distal cauda region, a weak and diffuse signal for TRPV6 was also seen in the cytosolic compartments. Vesicle-like structures in the luminal content were also observed, particularly in the regions of the initial segment, caput, and corpus epididymidum. No detectable immunoprecipitation for TRPV6 was seen in clear cells, basal cells, halo cells, muscle cells, or interstitial tissues of all regions of the epididymis, suggesting no protein expression in these cells. Western blot analysis using this antibody detected a major band at ~83 kD (corresponding to the expected size of TRPV6) in protein extracts from kidney, testis, caput, corpus, and cauda epididymides (Fig. 1 H). There were weak banks above the expected size of TRPV6, which may suggest that there are post-translational modifications of TRPV6, whereas the weak banks below the expected size might represent its degradation products. The immunolabeling of TRPV6 in principal cells was abolished when the antibody had been preabsorbed with an excess amount of the immunizing peptide from the manufacturer, confirming specificity of the antibody (Fig. 1, I and J).

Passive membrane properties of single epididymal epithelial cells

The enzymatic dispersion of rat cauda epididymis consistently yielded healthy epithelial cells (Fig. 2 A), and the passive membrane properties were obtained readily using the whole-cell patch-clamp method described in Materials and methods. Immunofluorescence staining of isolated epithelial cells provided evidence that the cells positively stained for TRPV6 exhibited morphological features consistent with those of principal cells (Fig. 2, B and C). The epididymal epithelial cells (presumably the principal cells) were usually identified by
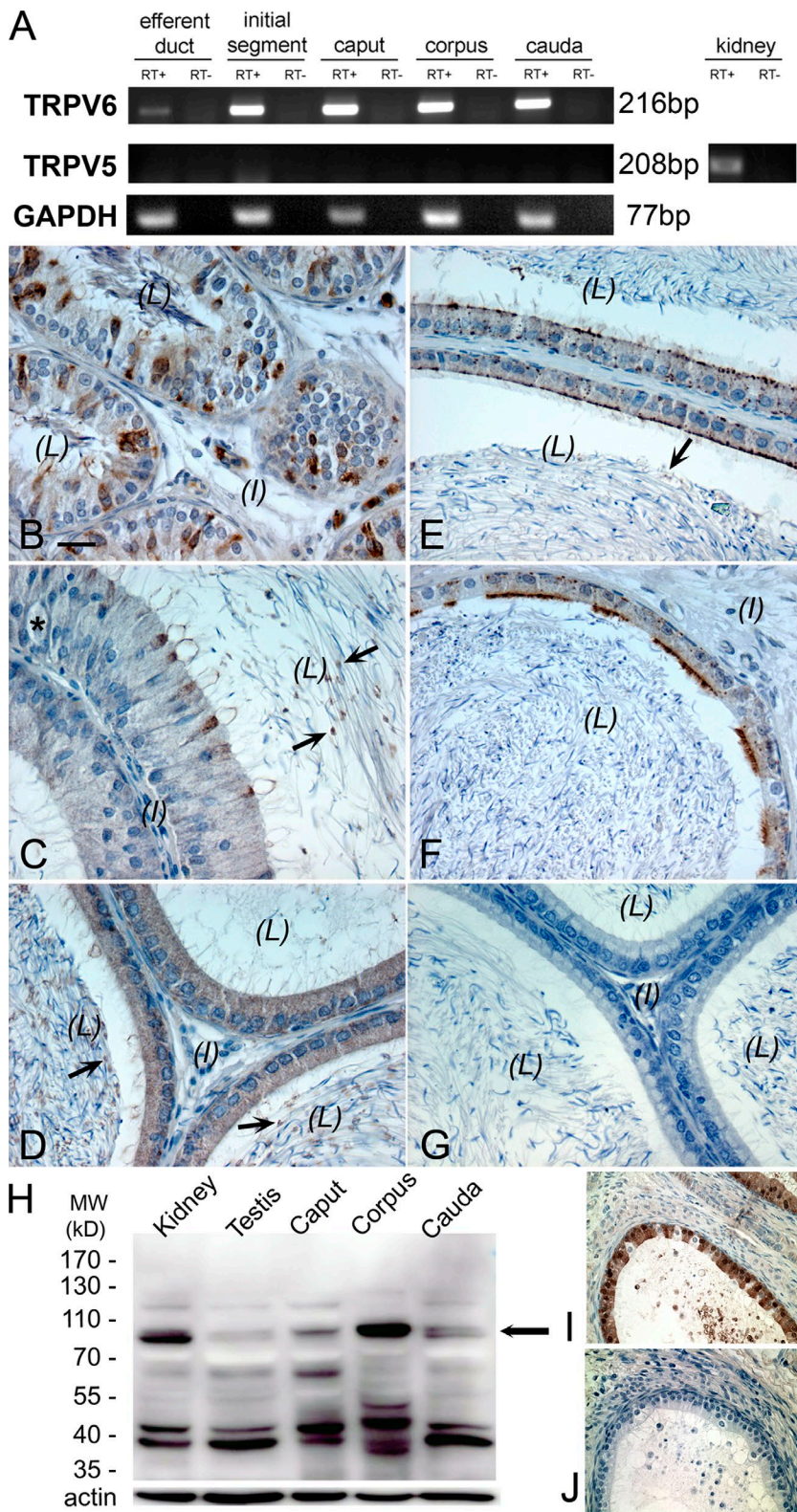
Figure 1. **Cellular localization of epithelial Ca²⁺ channel TRPV6 along the male excurrent duct.** (A) RT-PCR detection of mRNA for TRPV6 in the rat efferent duct and the different regions of epididymis, including the initial segment and caput, corpus, and cauda epididymides. No TRPV5 mRNA was detected in these tissues (except in the kidney, which was used as a positive control). RT+, PCR products with RNA sample templates; RT−, no RNA template control. GAPDH, glyceraldehyde 3-phosphate dehydrogenase. (B–G) Immunoperoxidase detection of TRPV6 protein (brown) in the rat efferent duct (B), initial segment (C), caput (D), corpus (E), and cauda epididymides (F). Negative control for immunohistochemistry without primary antibody showed no brown immunoperoxidase product (G). Arrows indicate the vesicle-like structures in the luminal content; the asterisk in C indicates a halo cell. *L*, lumen; *I*, interstitial tissue. Bar, 20 μm. (H) Western blot detection of TRPV6 protein (~83 kD, arrow) using the same antibody in total homogenates as indicated. MW, molecular weight. (I and J) Specificity of the TRPV6 antibody was confirmed by the absence of immunoprecipitation after immunopeptide preabsorption.

their larger size, with a rough microvilli on one end and polarized distribution of intracellular contents. These features suggested that the cells retained much of their cellular polarity after cell isolation and during the patch-clamp experiments. Other cells may include basal cells and clear cells; whereas the former group of cells was believed to be those possessing neither prominent microvilli nor polarized cellular contents, the latter group of cells might be those possessing some microvilli and polarized cell contents.
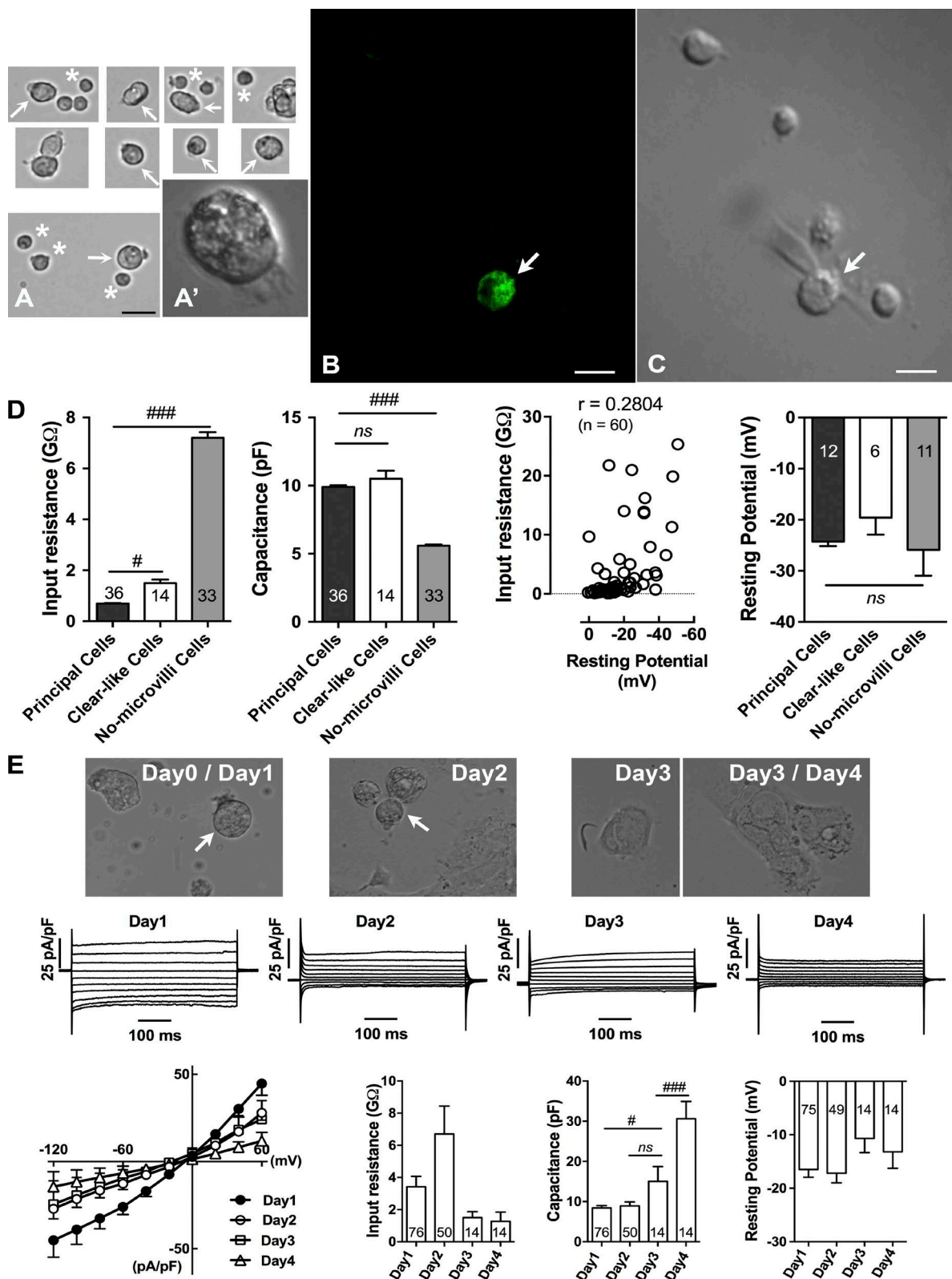
Figure 2. **Passive membrane properties of single epididymal epithelial cells.** (A) Examples of epithelial cells isolated from rat cauda epididymis after being reharvested from overnight culture on a dish before patch-clamp experiments. Only single cells were selected for patch-clamp recording. Arrows indicate epididymal epithelial cells (presumably principal cells or clear-like cells), and asterisks indicate no-microvilli cells, from which patch-clamp recordings were also done but the data were not presented. Insets show polarized distribution of intracellular contents in a principal cell. (B) Immunofluorescence detection of TRPV6 in fixed isolated epithelial cells showing typical example of a cell sharing the features of principal cells with positive staining (arrow). (C) Transmitted

Primary epithelial principal cells were further distinguished by their distinct passive membrane properties using the whole-cell patch-clamp technique (Fig. 2 D). Cell capacitance and input resistance were calculated from the current response to a 10-mV hyperpolarizing step applied from a holding potential of −60 mV as long as the whole-cell configuration was established when the giga ohm seal was achieved. The capacitance is directly related to membrane surface area (specific membrane capacitance is ~1 $\mu F/cm^2$), whereas the input resistance measured at these potentials is indicative of the intrinsic membrane or "leak" conductance. Principal cells exhibited passive membrane properties as well as current patterns that were significantly different from other cell groups, as described in the subsequent sections. Their mean input resistance and cell capacitance values of 0.7 ± 0.1 GΩ and 9.9 ± 0.7 pF, respectively (n = 36). In cells that also possessed polarized cellular contents and some microvilli, which were believed to be clear cells and are termed clear-like cells in this paper, had significantly different input resistance values (1.5 ± 0.5 GΩ; n = 14; P < 0.05), although there was no significant difference in capacitance values compared with principal cells (10.5 ± 2.2 pF; n = 14). These clear-like cells showed different responses to the alteration of extracellular pH and changes in holding potentials and testing voltage pulses, and they could be readily differentiated from the principal cells described in the subsequent section by these differences in response. Another group of cells, termed no-microvilli cells, which might include basal cells, also possessed distinct current patterns different from those of the principal cells and clear-like cells, and their mean input resistance was measured as 7.2 ± 1.3 GΩ and capacitance as 5.6 ± 0.5 pF (n = 33; P < 0.001). The larger cell capacitance value in principal cells suggested that microvilli increase the cell surface area, whereas the low input resistance might reflect the intrinsic leak conductance of principal cells. It is worthwhile to note that the input resistance of principal cells was resumed (>10 GΩ) after blockade of the leaky current with the nonspecific cation channel blocker lanthanum ($LaCl_3$ or La^{3+}).

The resting membrane potential was determined under current clamp as the zero-current potential, shortly after establishing the whole-cell configuration, using a low EGTA potassium-gluconate pipette. In whole-cell recordings, the leak conductance across the membrane and at the seal between the membrane and pipette both contributed. It is usually assumed that the seal has a much higher resistance than the membrane, ensuring that it has minimal influence on the measurement of membrane potential. In this study, the observed low input resistance in epithelial cells might have reflected a low seal resistance, and some membrane potentials were less polarized at lower values. However, correlation analysis of input resistance with resting membrane potential in all cells gave a value of ~0.28 (n = 60), showing a weak influence of input resistance on the measured resting membrane potential (Fig. 2 D). In addition, we did observe a low input resistance of 0.7 GΩ correlating with a resting potential as low as −38 mV, compared with the mean resting potential of all cells of approximately −24 mV. Resting membrane potentials were therefore reported only from cells with an input resistance 0.7 GΩ or more. There was no obvious difference on the measured resting membrane potential among the different cell groups (Fig. 2 D). The resting potentials of principal cells, clear-like cells, and no-microvilli cells were −24.3 ± 3 mV, −19.6 ± 8.1 mV, and −25.9 ± 11 mV, respectively.

Cell capacitance and current patterns differed significantly when cells were cultured for a few days (Fig. 2 E). Day 0 and day 1 cells were morphologically similar in shape and size. On day 2, some of the cells maintained their shape and size while some of them spread out; however, their current densities were significantly smaller than that on day 1, particularly the inward currents at negative potentials. On day 3 and day 4, the cell capacitance was significantly larger; accompanying cells became spread out, and their current patterns were much smaller than those recorded on day 1. The mean resting potentials were not significantly different than those measured at different time points but were slightly depolarized in later days. Therefore, only subsequent patch-clamp results from day 1 are reported in order to make consistent comparisons.
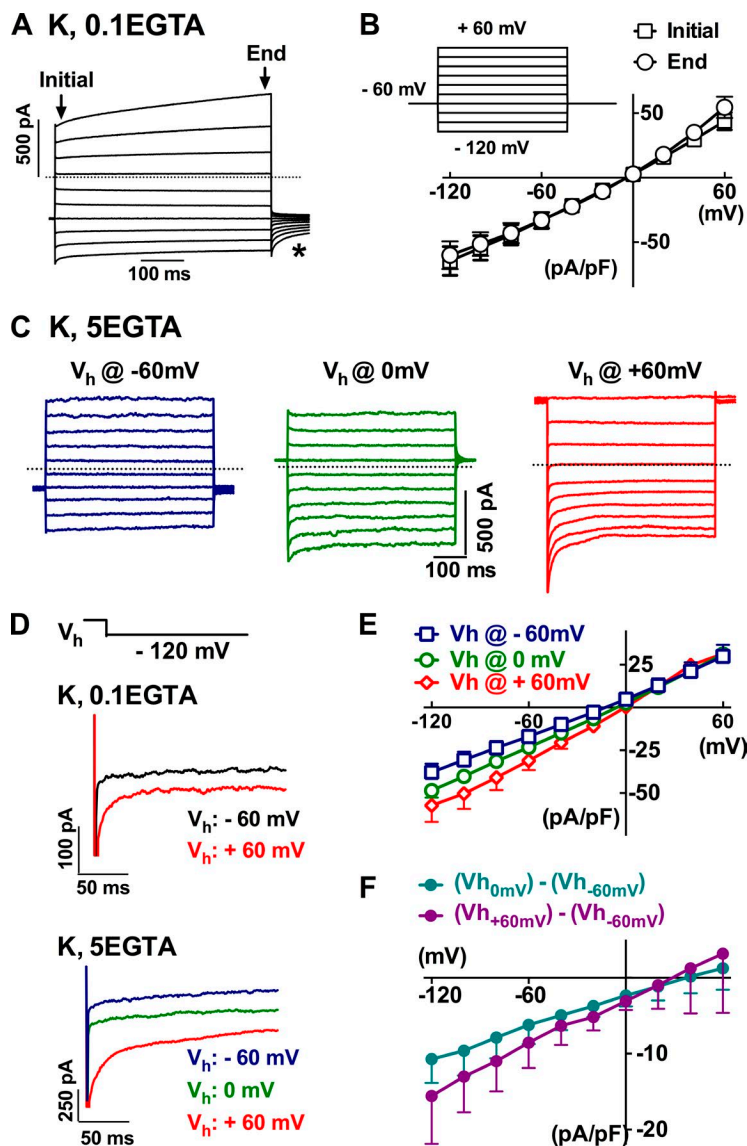
Constitutively active TRPV6-like conductance in whole-cell currents of principal cells

Current component is sensitive to changes in membrane voltage potential in K⁺-filled cells. Under quasiphysiological conditions with cells bathed in normal PSS and dialyzed with a low-calcium buffering potassium-based pipette solution, several current components were recorded by stimulating principal cells from a holding potential of −60 mV to a series of 500-ms testing voltages ranging from −120 to 60 mV (Fig. 3, A and B). The applied voltage steps instantaneously induced changes in

light microscopy image of the same cells (arrow). (D) Passive membrane properties of single rat epididymal cells as shown in A. (E) Images showing examples of principal cells isolated from rat cauda epididymis after day 0–4 cultures. Arrows indicate the identified principal cells in earlier culture days, whereas on later days, cells showed very different morphology. The typical current patterns and corresponding I-V plots as well as the membrane properties in different culture days are also shown. Numbers of cells tested are shown within bars. #, P < 0.05; ###, P < 0.001; ns, no significant difference versus appropriate controls using one-way ANOVA with Bonferroni post-hoc test. Bars: (A) 20 μm; (B and C) 10 μm. Error bars represent SEM.

Ion channel coupling in epithelial ion transport | Gao et al.

A K, 0.1EGTA

B

Figure 3. **Whole-cell currents in single epididymal epithelial cells.** (A) Typical whole-cell currents recorded from single epididymal epithelial cells when bathed in normal PSS and dialyzed with 0.1 mM EGTA potassium-based pipette solution (K, 0.1 EGTA) using a pulse-eliciting protocol as in the inset in B. The asterisk indicates the tail current. The dotted line (herein and in the subsequent figures) indicates the zero current level. (B) The current–voltage relationship of the currents from the epithelial cells as in A. (C–E) The current response recorded with a dialyzing pipette solution of strong intracellular Ca^{2+} buffering with 5 mM EGTA at holding potentials of −60, 0, and 60 mV. (F) Digitally subtracting the currents recorded at holding potential of −60 mV from that at 0 or 60 mV gave inwardly rectifying currents with a reversal potential proximately close to 30 mV. Error bars represent SEM.

C K, 5EGTA

D

E

F

outward and inward currents followed by time-dependent activation at positive potentials and inactivation at negative potentials, accompanied by a tail current upon cell repolarization (Fig. 3 A, asterisk). The total current at the beginning of the tested positive potential pulses (e.g., activating at 60 mV) was slightly smaller than that at the end of the pulses, but it was larger at the beginning of negative potentials (e.g., decaying or inactivating at −120 mV; Fig. 3 B; $n = 9$).

A designated set of experiments using Na-gluconate and Cs-methansulphonate as the major ions in the extracellular and internal pipette solutions to suppress K^+ and Cl^- conductance and high BAPTA was included in the pipette to suppress other Ca^{2+}-dependent components in order to confirm the presence of constitutive activity of TRPV6 channels in isolated primary principal cells. It was found that primary principal cells still exhibited prominent currents under these recording conditions, indicating that the basal nonspecific leak current was not sensitive to the internal Cs^+ ions and the depletion of intracellular Ca^{2+} by 10 mM BAPTA (Fig. 4). In the presence of magnesium (Fig. 4 A), an increase in the extracellular calcium concentration from 0 or 2.5 mM to 30 mM dramatically increased the current response measured at −80 mV membrane potential. The subsequent change in Ca^{2+} concentration from zero level to 2.5 mM initially induced a current, which was almost run down after prolonged presence of the extracellular Ca^{2+}, consistent with the autoinhibition effect caused by extracellular calcium on TRPV6 channels. When the divalent cations were removed from the extracellular solution, the current (Fig. 4 B), mainly caused by Na^+ conductance, was initially decreased but then dramatically increased. This stable monovalent current was reversible and diminished in the presence of divalent cations.

The subtraction of the current responses to the voltage ramp applied under dictated conditions between
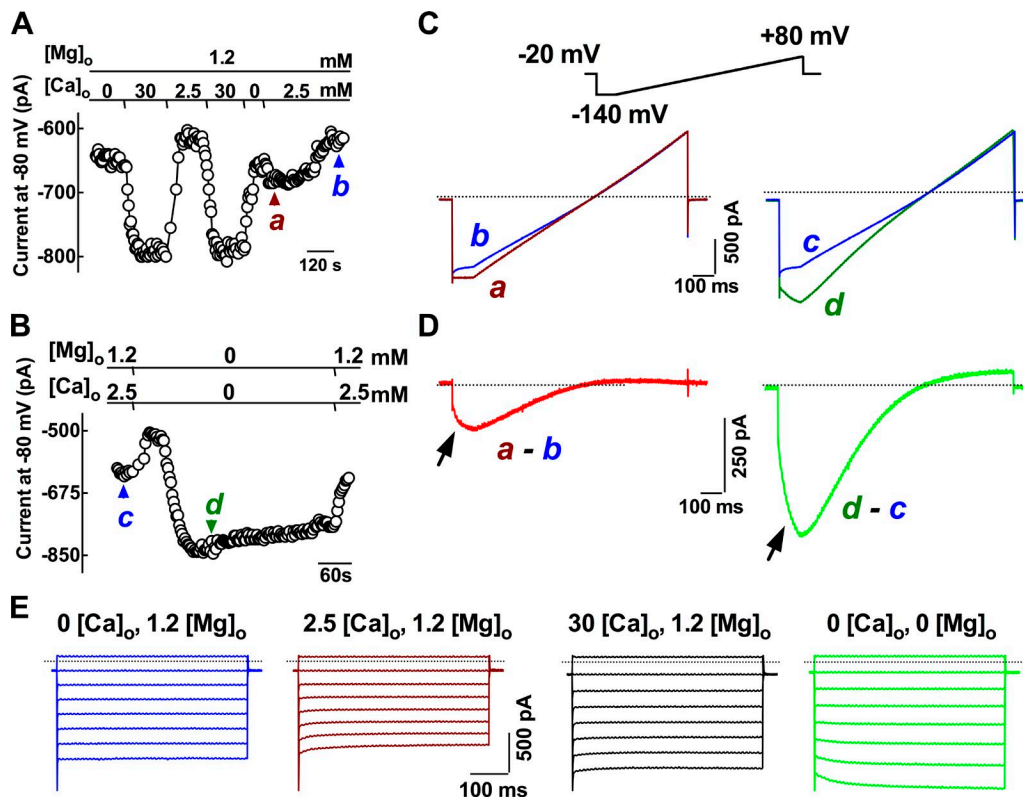
Figure 4. **Constitutive electrophysiological activity of TRPV6-like current in principal cells: inwardly rectifying Ca²⁺-selective and monovalent conductance.** (A) Time course of the current changes recorded at different extracellular Ca²⁺ concentrations ([Ca²⁺]$_o$). The current was initially recorded in a nominally Ca²⁺-free solution. Increasing [Ca²⁺]$_o$ to 30 mM reversibly evoked a current, which was attenuated in 2.5 mM Ca²⁺-containing solution. When increasing [Ca²⁺]$_o$ from nominally Ca²⁺-free solution to 2.5 mM Ca²⁺-solution, a small inward current was evoked, which was then followed by an almost complete rundown. (B) A monovalent cation current was revealed when switching the normal external solution to a divalent (Ca²⁺ and Mg²⁺) cation-free saline. (C and D) Current–voltage ramps recorded at the time points as indicated in A and B, and current–voltage curves were digitally subtracted from different conditions as indicated. The subtracted currents showed inwardly rectifying at negative potentials. Arrows indicated the negative slopes of current responses at the hyperpolarization step before the applied voltage ramp. Dotted lines indicate the zero current levels. (E) Typical tracings showing the current kinetics at negative potentials in different ionic conditions. Tested pulses were applied from a holding potential at 0 mV to a series of 500-ms steps between 20 and −120 mV in 20-mV intervals. Bathing fluid low chloride Cs-PSS and low chloride Cs-based pipette solutions were used for recording.

−140 and 80 mV from a holding potential of −20 mV revealed inwardly rectifying currents at negative potentials (Fig. 4, C and D), and the current response was more prominent in the divalent-free condition and exhibited a negative slope at the beginning of strong hyperpolarization before the voltage ramping up (Fig. 4 D, arrows). The current responses at hyperpolarizing steps showed decaying kinetics only in the presence of Ca²⁺ and Mg²⁺ in the extracellular solution (Fig. 4 E). The current kinetics was steady during the 500-ms voltage steps when cells were exposed to a Ca²⁺-free with Mg²⁺ in the bating solution. The addition of 2.5 mM Ca²⁺ to the bathing solution caused the current responses to decay with time during the hyperpolarizing voltage pulses. A further increase in Ca²⁺ to 30 mM counteracted the decaying kinetics, whereas the divalent-free conditions converted the time-dependent decaying kinetics to activating during the 500-ms hyperpolarizing steps.

CaCC activity and expression of TMEM16A in epididymal principal cells

In view of the presence of inward-rectifying TRPV6-like conductance, which contributes only the inward currents at hyperpolarizing potentials, and the time-activating conductance at depolarizing steps in primary principal cells, which was not suppressed when cells were dialyzed with a Cs⁺-filled pipette solution and bathed in normal PSS (data included in Fig. 5 B*e*), it was therefore hypothesized that CaCC activity was also present in the whole-cell currents of these principal cells, in addition to the TRPV6 channels. To confirm this notion, the putative CaCC blocker niflumic acid was used. It was found that the whole-cell currents of principal cells were significantly attenuated by niflumic acid even at 10 µM (Fig. 5 A). Cells were bathed in normal PSS and dialyzed with potassium-based pipette with minimal intracellular calcium buffering capacity. In the presence of 100 µM niflumic acid, the current components with time-depen-
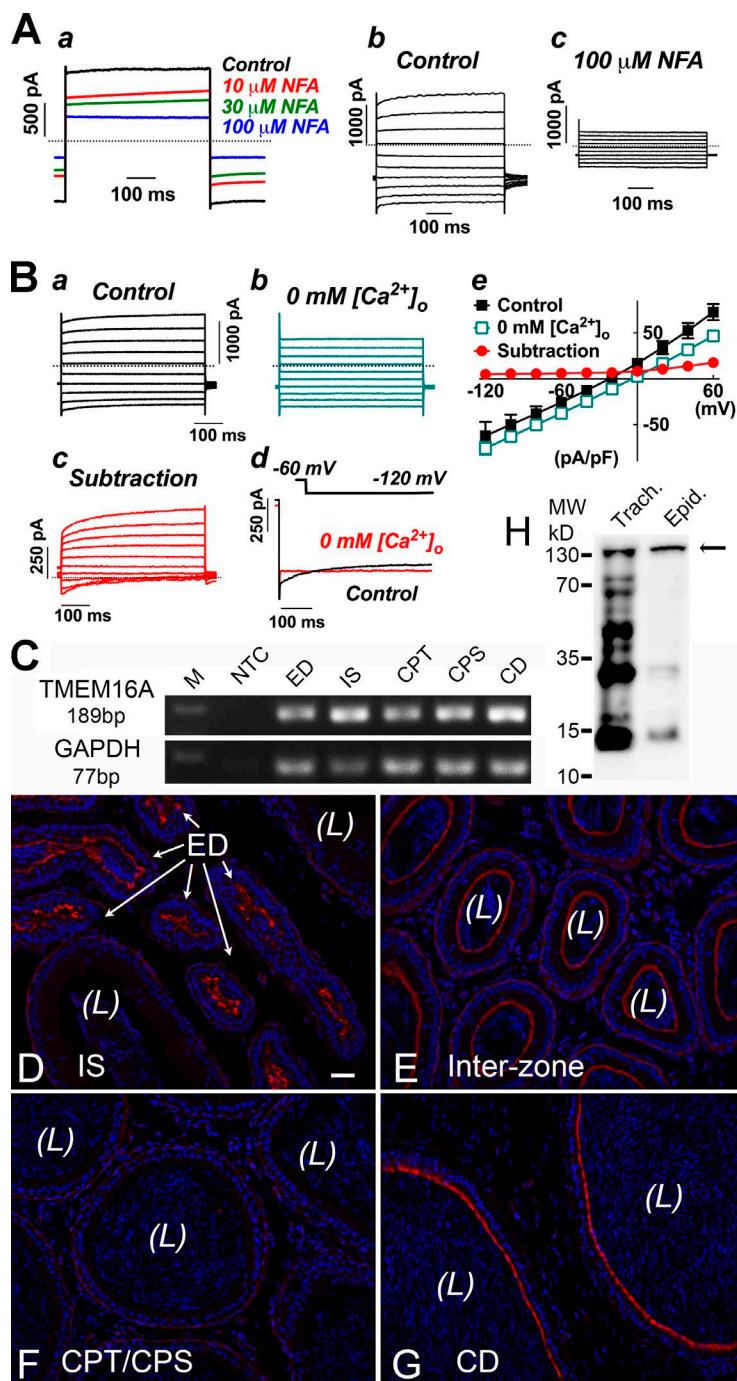
Figure 5. **Functional activity and expression of calcium-activated chloride channel TMEM16A in epididymal principal cells.** (Aa) Whole-cell current of a principal cell showing sensitivity toward the putative CaCC blocker niflumic acid (NFA; 10–100 µM). Currents were in response to the repeatedly applied depolarizing episodes from a holding potential of −60 to 60 mV. Bath solution was normal PSS, and pipette solution was K$^+$ based with 0.1 mM EGTA. (Ab and Ac) Typical current tracing from a principal cell in response to a series of 500-ms, 20-mV increment voltages steps applied between −120 and 60 mV evoked from the holding potential −60 mV before (Ab) and after (Ac) the addition of 100 µM niflumic acid. (B) Current responses of a principal cell obtained in the control condition with 2.5 mM Ca^{2+} in the bathing solution (Ba) and in the nominally extracellular Ca^{2+}-free condition (0 mM [Ca^{2+}]$_o$; Bb). The dialysed pipette solution was K$^+$ based with 0.1 mM EGTA. (Bc) The subtraction revealed that the extracellular Ca^{2+}-sensitive currents were mainly the outwardly rectifying current with time-dependent activating kinetics at positive potentials as well as a small transient decaying current at negative potentials. (Bd) Current tracings recorded from a principal cell in response to a hyperpolarizing step from −60 to −120 mV before and after removal of extracellular Ca^{2+}. Dotted lines indicate the zero current levels. (Be) I-V plots for the conditions as described in Ba–Bc. Data were measured at the end of testing pulses. Error bars represent SEM. (C) Conventional RT-PCR detection of the TMEM16A mRNA in the rat epididymis and efferent duct. CD, cauda epididymides; CPS, corpus; CPT, caput; ED, efferent duct; GAPDH, glyceraldehyde 3-phosphate dehydrogenase; IS, initial segment; M, marker; NTC, no template control. (D–G) Confocal immunofluorescent images showing the localization of TMEM16A protein (red) in the apical pole of principal cells of the rat interzone and cauda epididymides and in the ciliated cells of the efferent duct. Weak immunoreactivity was also detected in smooth muscle cells and in some interstitial cells, but negligible immunoreactivity was detected in principal cells of the caput and corpus epididymis. (H) Western blot detection of TMEM16A protein using the same antibody for immunofluorescent labeling in the crude protein extracts from rat trachea (Trach.) and epididymis (Epid.). The DNA of epithelial cells and sperm is labeled with DAPI in blue. L, lumen. Bar, 50 µm.

dent kinetics at both positive and negative potentials were inhibited, leaving the time-independent residual currents during the 500-ms testing pulses. The current density at 60 mV, as measured at the end of testing pulses, decreased from an initial value of 78.3 ± 15.2 to 22.5 ± 5.2 pA/pF (P < 0.05) in the presence of 100 µM niflumic acid, and the density at −120 mV decreased from −101.8 ± 29.2 to −42.8 ± 10.0 pA/pF, corresponding to 67 ± 11 and 49 ± 16% of total currents at respective testing pulses (n = 3). The inhibitory effect of niflumic acid was quickly reversible (unpublished data).

However, the reversal potential determined from the I-V curves showed no significant alteration in the presence of niflumic acid (from −5.3 ± 1.7 to −6.3 ± 1.1 mV; n = 3).

Removal of Ca^{2+} from the bathing solution in the presence of Mg^{2+} consistently and significantly attenuated the time-dependent components of principal cells (Fig. 5 B, a and b). The attenuated components comprised a prominent outward current with depolarization-activating kinetics at the positive testing pulses as well as a small inward current with hyperpolarization-activated decaying kinetics at the negative potentials

(Fig. 5 B, c and d). The extracellular Ca^{2+}-dependent currents, obtained by subtracting the currents recorded under the nominally Ca^{2+}-free condition from that of the control condition, revealed a prominent outwardly rectifying current and a small inward transient current component at strong hyperpolarizing potentials (Fig. 5 B, c–e). The internal pipette solution was either K^+ filled or Cs^+ filled, with low internal Ca^{2+} buffering (i.e., 0.1 mM EGTA). The current amplitude measured at the end of the depolarizing pulse to 60 mV was decreased by $46 \pm 10\%$, from 72.7 ± 10.2 to 39.8 ± 9.6 pA/pF ($P < 0.05$; $n = 4$). The decaying current component at hyperpolarizing potentials (between −80 and −120 mV) disappeared in the nominally Ca^{2+}-free condition; however, the current amplitude was slightly enhanced. As measured at the end of the 500-ms testing pulse of −120 mV, the mean current density changed from $−62.1 \pm 17.5$ pA/pF for the control to $−75.9 \pm 8.0$ pA/pF ($n = 4$) in the calcium-free solution. Noteworthy is that the reversal potential as determined from the IV plots was significantly depolarized after the removal of calcium ions from the bathing solution (from $−19.2 \pm 1.3$ to $−5.7 \pm 3.2$ mV; $P < 0.01$, paired t test; $n = 4$).

The expression of CaCC channel candidate TMEM16A mRNA in the rat epididymis was first confirmed using conventional RT-PCR (Fig. 5 C). All PCR experiments were reproducible in separate RT-PCR reactions using the total RNA extracts from three animals. The expression of TMEM16A protein was then examined on paraformaldehyde-lysine-periodate (PLP)–fixed rat epididymis cryostat sections using a rabbit polyclonal anti-TMEM16A antibody and immunofluorescence confocal microscopy method. The cellular localization of TMEM16A protein was confirmed to express in the apical membrane of principal cells in the rat cauda epididymis as well as in ciliated cells of the efferent duct (Fig. 5, D–G). A prominent immunofluorescent signal for TMEM16A was also detected in the apical membrane of principal cells of the intermediate zone, cauda epididymis, and vas deferens, but not principal cells of the initial segment, caput, and corpus epididymidum. Weaker labeling was also observed in some interstitial cells as well as the smooth muscle cells surrounding the epididymal tubules of the initial segment, caput, and corpus regions. Western blot analysis showed a major band at ∼130 kD for both protein extracts from rat epididymis and positive control trachea (Fig. 5 H). The molecular size is higher than the expected size for TMEM16A at 119 kD, indicating potential posttranslational modification of TMEM16A. The bands at lower molecular weight could be the degradation products of TMEM16A, which is more prominent in trachea than in epididymis, suggesting faster turnover of TMEM16A in the trachea.

Lanthanum-inhabitable currents revealed TRPV6-like and TMEM16A-like activities in single epididymal epithelial cells

The extracellular application of lanthanum ($LaCl_3$ or La^{3+}; 200 µM), a putative blocker of nonspecific cation channels, revealed that there were at least three different kinds of current components that were sensitive to the inhibition by lanthanum in different time courses (Fig. 6). There was a current component measured at −60 mV that was instantly inhibited by La^{3+} (Fig. 6 A, red open arrow), a current component at 60 mV that was attenuated in a slower manner (Fig. 6 A, blue open arrow), and a third current component that was diminished after the attenuation of the secondary component (Fig. 6 A, double arrow). The current component at negative potential that was instantly inhibited by lanthanum was more obvious during the responses toward the voltage ramp applied to the cells, and >80% of the current responses at negative potentials (i.e., between −40 and −120 mV) were inhibited within 10 s after the addition of lanthanum (Fig. 6 B, arrow), whereas only ∼50% of the current at positive potentials were inhibited at this time point (Fig. 6 B, double arrow). The currents at the positive potentials that were slowly inhibited had time-dependent activating kinetics during the 500-ms depolarizing episodes from −60 to 60 mV (Fig. 6 C). This characteristic current component was not sensitive to the replacement of potassium-gluconate in the pipette solution with Cs-methanesulfonate (unpublished data), suggesting that it might be a chloride current component and consistent with the notion of TMEM16A. The current–voltage relationship plots confirmed that in the early presence of lanthanum in the recording bathing fluid, the inward currents at the negative potentials were inhibited first, giving inwardly rectifying subtraction currents with positive reversal potentials of 36.4 ± 11.2 mV ($n = 4$), suggesting a current component resembling TRPV6 channel activities. However, after a prolonged presence of lanthanum, the total currents were almost abolished (Fig. 6, D and E). The effect of lanthanum was reversible, and the transient hyperpolarizing-induced decaying current at hyperpolarizing steps (i.e., −80 to −120 mV) as well as the depolarizing-induced activating current at depolarizing steps (i.e., 60 mV; Fig. 6 F, wash-off).

Effect of the TMEM16A inhibitor tannic acid on the membrane potential of isolated caudal epididymal cells

The interplay between TRPV6 and TMEM16A in the regulation of membrane conductance of principal cells was further examined by the effect of tannic acid, a specific inhibitor of TMEM16A, in the absence or presence of lanthanum, on the membrane potential of isolated epididymal cells. In Fig. 7 A (left), addition of 100 µM tannic acid triggered the cells to depolar-
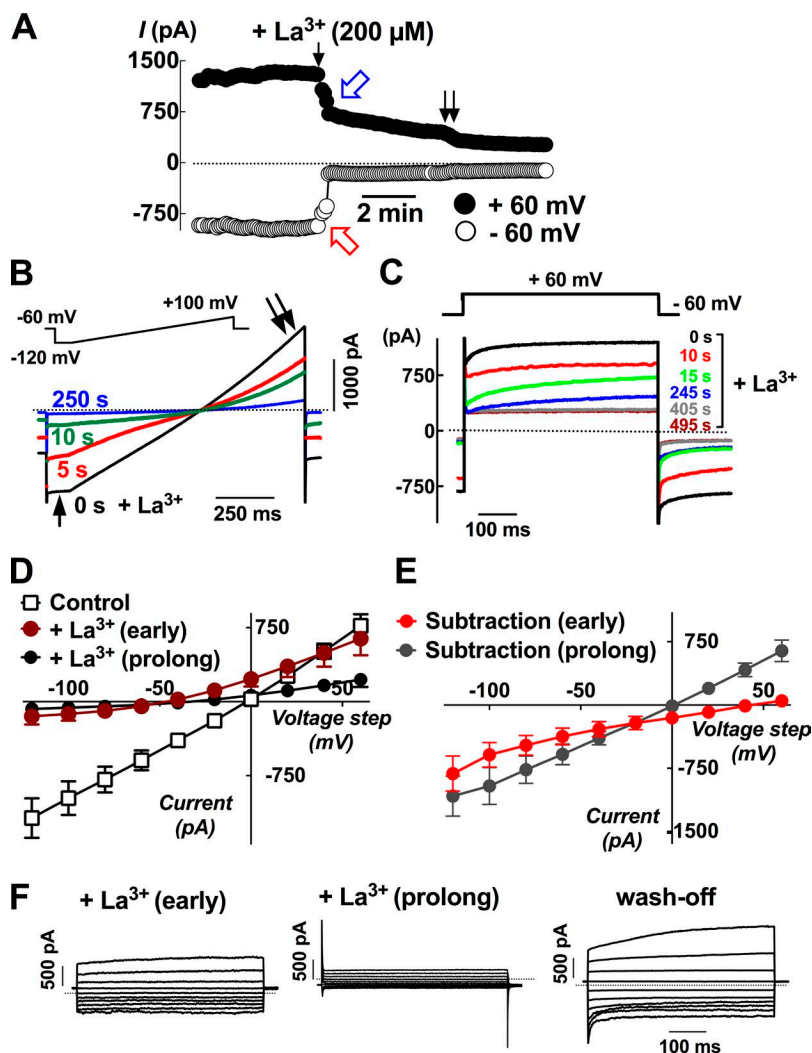
Figure 6. **Lanthanum-inhabitable currents revealed both TRPV6-like and CaCC current components in the same single epididymal cell.** (A) At least two constitutively active current components (blue and red arrows) in principal cells were inhibited in a time-dependent manner after the addition of 200 µM lanthanum (La^{3+}) to the recording chamber solution. Currents were sampled at 5-s intervals from a holding potential of −60 to 60 mV. The pipette solution was potassium based with 0.1 mM EGTA, and the bathing solution was standard PSS. The dotted line indicates the zero current levels. (B) Current responses toward the voltage ramp applied from −120 to 100 mV from a holding potential of −60 mV confirmed that lanthanum had a faster inhibitory effect on the inward current at negative potentials (arrow) than the outward current at positive potentials (double arrows). (C) The current responses toward the 500-ms depolarizing episodes from −60 to 60 mV before and after the addition of 200 µM La^{3+}. (D) Current–voltage plots for the current responses under control conditions or in the presence of lanthanum for a short period time (within ∼30 s) or after prolonged presence (>5 min). (E) Subtraction currents revealed that the current inhibited by the early presence of lanthanum was inwardly rectifying with a reversal potential at positive potential (subtraction early), whereas the total currents inhibited at the various voltages showed a linear relationship (subtraction prolonged). Error bars represent SEM. (F) Tracings showing the current responses toward the series of testing pulses between −120 and 60 mV in the early or prolonged presence or after wash-off of lanthanum.

ization, as indicated by the increase in fluorescence intensity ratio, whereas the subsequent addition of 100 µM La^{3+} to the same cells, hyperpolarization was observed. On the contrary, addition of lanthanum to the control cells caused significantly hypopolarization and the subsequent addition of tannic acid to these cells had no depolarization effect (Fig. 7 A, right). In Fig. 7 B are typical tracings showing that the depolarization response triggered by tannic acid was almost instant, whereas the hyperpolarization kinetics mediated by lanthanum was much slower. Fig. 7 C shows the summary of end-point measurements of the effect of tannic acid and lanthanum on membrane potential after cells were isolated and cultured for a few days. Consistent with the membrane property results shown in Fig. 2 E, the depolarization effect of tannic acid was only detected in cells on days 0 and 1, but not days 2 and 3. The hyperpolarization effect of lanthanum was also more prominent at day 0 and day 1 than on later days.

Cellular colocalization of TRPV6 and TMEM16A in principal cells of the epididymis

To determine the cellular colocalization of TRPV6 and TMEM16A, we performed double-immunofluorescent labeling of rat epididymis sections (Fig. 8). Our results showed that TRPV6 and TMEM16 colocalized in the apical pole of the intermediate zone and distal caudal epididymis. The colocalization was particularly found in granular structures at the apical pole of the intermediate zone of the epididymis and on the surface of sperm, as well as in the apical microvilli of principal cells in the cauda epididymis. No colocalization was observed in the regions of the initial segment, caput, and corpus epididymides.

Effect of alterations of extracellular pH on whole-cell currents and the Ca^{2+} influx in isolated epididymal principal cells

It is known that TRPV6 channel activity is sensitive to extracellular pH and that the lumen of epididymis is
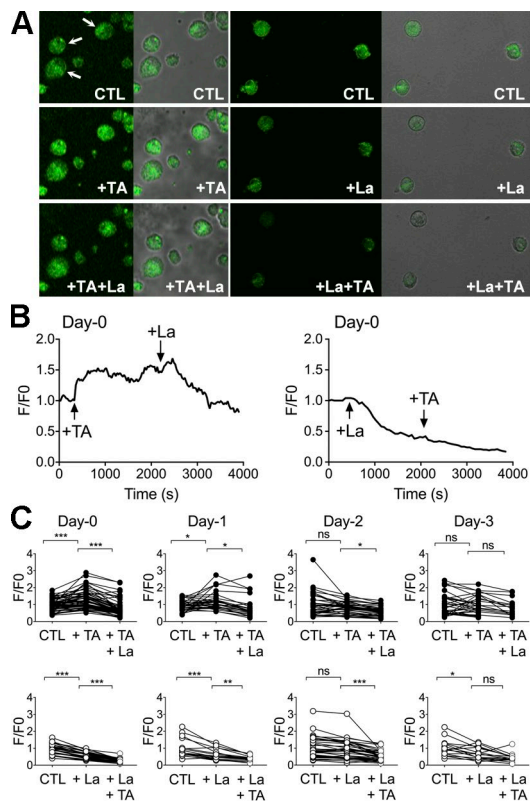
Figure 7. Effects of tannic acid and lanthanum on the membrane potential of isolated caudal epididymal principal cells. (A) Representative DiBAC4(3) fluorescence of single principal cells isolated from cauda epididymis of rats before (CTL, denoting the control condition) and after addition of 100 µM tannic acid (+TA; left) or 100 µM La^{3+} (+La; right) and the subsequent addition of either inhibitors. Arrows indicate the cells that would have been selected for measurement. (B) Typical tracings showing the fast depolarization triggered by tannic acid or the gradually hyperpolarizing response induced by La^{3+} on control cells. Subsequent addition of La^{3+} to TA-treated cells caused hyperpolarization, but pretreatment with La^{3+} prevented the depolarizing effect of TA. (C) Summary of the end-point effects of TA and La^{3+} (30-min treatment) on the membrane potential of principal cells from different culture days. *, $P < 0.05$; **, $P < 0.01$; ***, $P < 0.001$; ns, no significant difference (one-way ANOVA).

maintained at acidic pH. Therefore, it is worthwhile to test the sensitivity of whole-cell currents of principal cells toward alterations of extracellular pH (pH_o). Under quasiphysiological conditions (i.e., cells were dialyzed with potassium-pipette solution and bathed in normal PSS), changing the extracellular pH_o from 7.4 or 8.4 to an acidic 6.4 markedly decreased the whole-cell currents of principal cells (Fig. 9 Aa); a further decrease in pH_o to 5.4 caused a further reduction, whereas increasing the pH_o to 8.4 from 7.4 enhanced these currents. The effect of altering pH_o on whole-cell currents was reversible and did not affect the reversal potential of the IV plots (Fig. 9 Ab). The mean current densities of five principal cells, measured at the initial phase of the hyperpolarizing step to −100 mV, was reduced from

−148 ± 86 to −86 ± 47 pA/pF when changing the pH_o from 7.4 to 6.4 but was increased to −228 ± 137 pA/pF by switching the pH_o to 8.4, whereas at 60 mV, the current density was reduced from 91 ± 49 pA/pF at pH_o 7.4 to 54 ± 29 pA/pF at pH_o 6.4 and increased to 160 ± 94 pA/pF at pH_o 8.4 (Fig. 9 Ad). Inclusion of 5 mM EGTA in the pipette solution to suppress Ca^{2+}-activated currents and replacement of extracellular K^+ ions with Cs^+ ions to remove any inward-rectifying potassium conductance did not affect the pH_o-sensitive currents, which were still persistent and reversible (Fig. 9 B). When the cations were replaced with NMDG in solutions on both sides and extracellular Ca^{2+} was presumably the only permeable cation, the whole-cell currents of principal cells were significantly run down (Fig. 9 Ca). However, there still remained a tiny current response that was enhanced by switching the acidic fluid at pH_o 6.4 to 7.4, and the subtraction of the pH-sensitive response revealed only the inwardly rectifying current at negative potentials (Fig. 9 C, b and c). The mean current densities at pH_o 7.4 were −1.9 ± 0.4 pA/pF at −120 mV and 2.7 ± 0.8 pA/pF at 60 mV ($n = 3$), corresponding to only 6 and 11% of the responses of principal cells when dialyzed with a potassium-based 5 mM EGTA pipette and bathed in Cs-PSS fluid, whose current densities were −31.6 ± 11.2 pA/pF at −120 mV and 24.8 ± 7.3 pA/pF at 60 mV (Fig. 9 B, c and d; $n = 5$), respectively. As shown in Fig. 9 (Ac, Ba, and Cb), the pH_o-sensitive current consistently contained a time-dependent decaying component at hyperpolarizing steps under the various ionic conditions, consistent with the feature of autoinhibition by extracellular calcium of TRPV6.

The Ca^{2+} selectivity and extracellular pH dependence of the TRPV6 channel together with its constitutive activity lead to the notion that the resting intracellular Ca^{2+} concentration ($[Ca^{2+}]_i$) of the isolated principal cells might be dependent on the extracellular concentration of Ca^{2+} ($[Ca^{2+}]_o$) and pH_o. This was confirmed using confocal imaging of intracellular calcium levels in Fluo-3–loaded principal cells (Fig. 9 D). Switching of normal PSS, pH_o 7.4, to a Ca^{2+}-free PSS with 1 mM EGTA caused a decrease in $[Ca^{2+}]_i$. Addition of 30 mM Ca^{2+} to the bathing fluid containing zero-Ca^{2+} resulted a remarkable increase in $[Ca^{2+}]_i$ to approximately fourfold that of initial levels. In the presence of 2.5 mM $[Ca^{2+}]_o$, increasing the pH_o to 8.4 from 7.4 reversibly increased $[Ca^{2+}]_i$, but decreasing the pH_o to 6.8 decreased $[Ca^{2+}]_i$ levels in isolated principal cells.

Ca^{2+} absorption in microperfused rat cauda epididymis
The rat cauda epididymis was perfused with 1 mM Ca^{2+}-containing bicarbonate-buffered (HCO_3) Krebs solution at a rate of ~1 µl/min, and the calculated rate of Ca^{2+} reabsorption was 2.6 ± 0.1 nmol/cm^2/min ($n = 16$ rats) at pH 7.4. There was no significant difference in the reabsorptive rate using HCO_3- or HEPES-buff-

Ion channel coupling in epithelial ion transport | Gao et al.
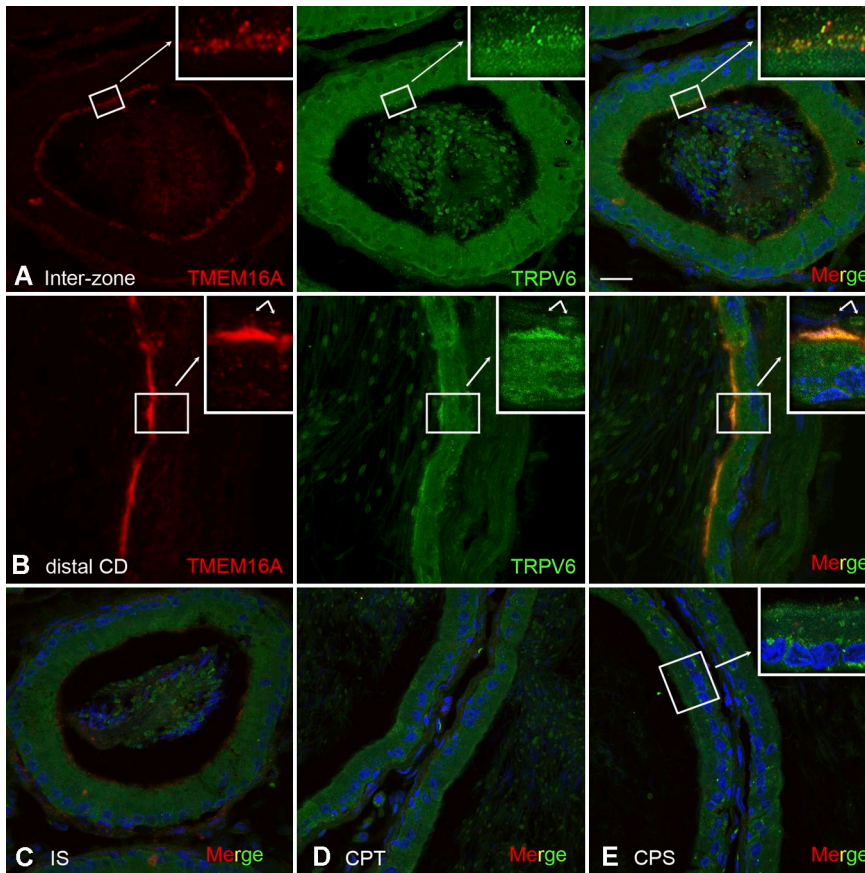
Figure 8. **Colocalization of TMEM16A and TRPV6 in epididymal principal cells.** (A and B) Confocal projections of serial stack images showing the double-immunofluorescent labeling for TMEM16A (red) and TRPV6 (green). The merged panels show that TMEM16A colocalizes with TRPV6 in the apical membrane of principal cells (yellow) in the cauda epididymis and in the vesicle-like structures in the apical pole of intermediate zone (interzone) and on the surface of sperm (arrows; B, insets). (C–E) No colocalization was observed in the initial segment (IS), caput (CPT), and corpus (CPS) epididymis. Nuclei were counterstained with DAPI in blue. Bar, 20 µm.

ered solution (Fig. 10 A), whereas it was enhanced by increasing the luminal Ca^{2+} concentration from 1 to 2 mM, increasing from 3.9 ± 0.2 to 8.5 ± 0.7 nmol/cm^2/min ($n = 5$ rats), whereas decreasing the luminal Ca^{2+} from 1 to 0.5 mM gave a significantly lower value (Fig. 10 B). Inclusion of 100 µM La^{3+} or the putative Ca^{2+} signaling channel blocker ruthenium red reversibly inhibited the rate of Ca^{2+} reabsorption by the rat cauda epididymis when using a HEPES-buffered Krebs at pH 7.4 (Fig. 10, C and D). The calculated IC_{50} using Prism software is ~115 µM (Fig. 10 E). Altering pH of the luminal perfused solution affected the rate of Ca^{2+} reabsorption by the rat cauda epididymis, and the rate was attenuated by changing the perfusing solution from pH 7.4 to 6.8 but was enhanced when changed to pH 8.2 (Fig. 10 F).

DISCUSSION

This study presents an investigation of whole-cell currents in primary principal cells isolated from the rat cauda epididymis and reveals an electrical coupling between TRPV6 and TMEM16A that participates in calcium homeostasis of the male reproductive duct. Our understanding of TRPV6 channel function in native cells and tissues is limited despite the phenotypes of TRPV6-deficient mice with male fertility problems and

malfunctions in Ca^{2+} uptake in the epididymis and other epithelial organs. In addition, the functional partner of TRPV6 has not been clearly elucidated (Stoerger and Flockerzi, 2014). In the present study, a constitutively active current with many properties of classical TRPV6 currents was found in the primarily native principal cells of the epididymis. Moreover, the present results provide evidence that a constitutive TMEM16A conductance also contributes to whole-cell conductance in principal cells, in which TRPV6 and TMEM16A are colocalized at their apical membranes. Therefore, an interplay of these two channels would most likely play a significant role in Ca^{2+} homeostatic regulation in the epididymis.

Constitutive TRPV6 and TMEM16A conductance contributes to whole-cell currents of epididymal principal cells

Prominent inward and outward currents were recorded from isolated rat cauda epididymal principal cells using a whole-cell patch-clamp technique and ATP-containing K^+-filled electrodes under quasiphysiological conditions. Rundown of the current was negligible, and stable currents could be recorded for even more than 30 min. Whole-cell currents consisted of a small inactivating inward current that activated at negative voltages under minimal intracellular Ca^{2+} buffering (i.e., 0.1 mM
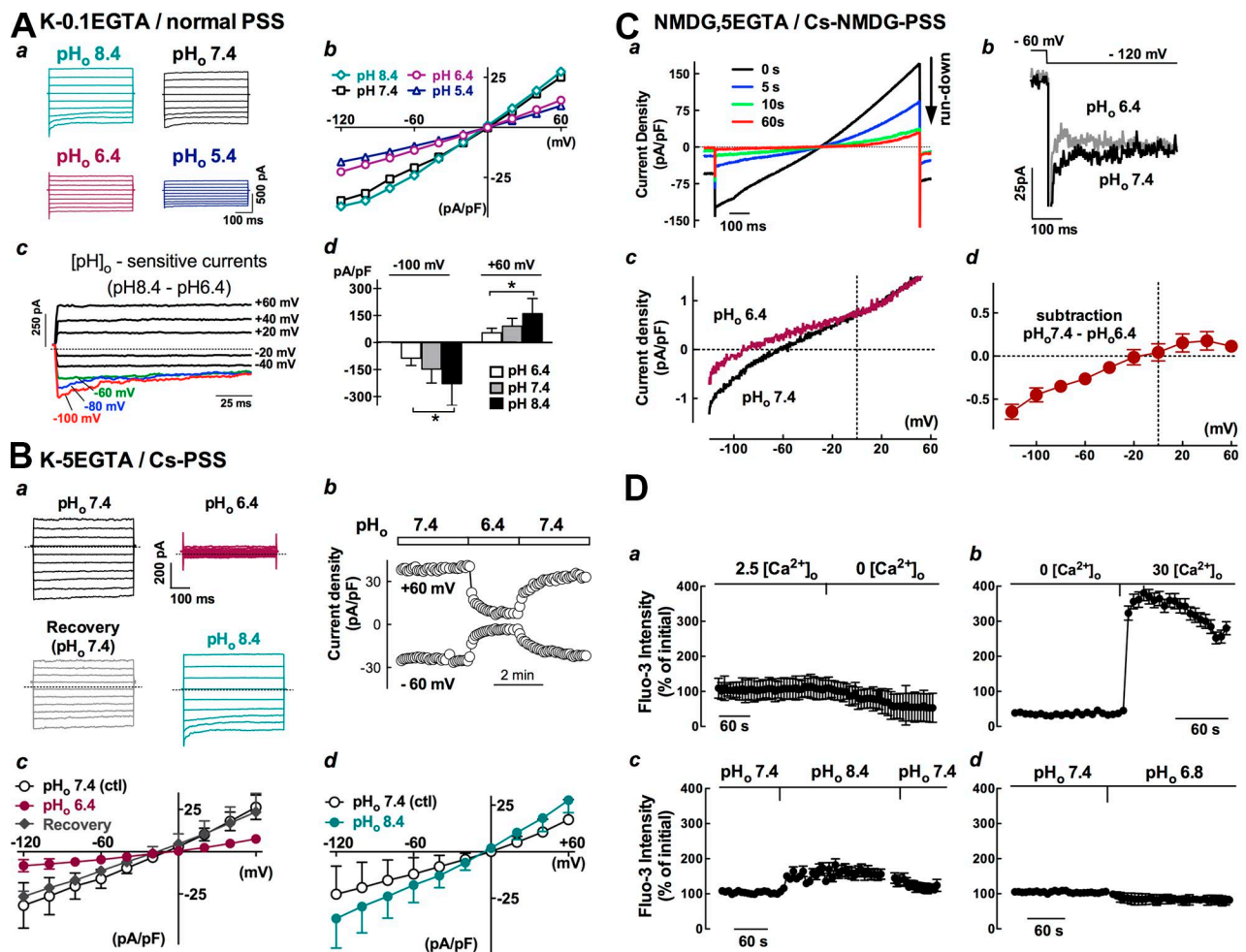
Figure 9. Changes of whole-cell currents and intracellular [Ca²⁺]ᵢ under different extracellular pH or ionic conditions in primary principal cells. (A–C) Whole-cell currents of principal cells were inhibited in acidic solution (pH₀ 6.4) but were enhanced in alkaline solution (pH₀ 8.4) under different ionic conditions. The holding potential was set at 0 or −60 mV. (A) The pipette solution was potassium-gluconate based containing 0.1 mM EGTA, and the bathing fluid was normal PSS (K-0.1 EGTA/normal PSS). The dotted line indicates the zero current levels. *, $P < 0.05$, one-way ANOVA. (B) The pipette solution was potassium-gluconate based containing 5 mM EGTA, and the K⁺ ions in bathing solution were replaced with Cs⁺ (K-5EGTA/Cs-PSS). (C) The major cation in both the pipette and the bathing solutions was replaced with NMDG, and the K⁺ in bathing fluid was replaced with Cs⁺ (NMDG, 5EGTA/Cs-NMDG PSS). All pipette solutions contained 3–4 mM ATP. (D) Changes in intracellular Ca²⁺ concentration ([Ca²⁺]ᵢ) when isolated rat cauda epididymal cells were loaded with Fluo-3-AM fluorescence dye. Fluorescence intensity was measured using a confocal imaging system. Data were obtained from at least 10 cells in three separate experiments. Error bars represent SEM.

EGTA). However, this small inward current became larger when the intracellular Ca²⁺ buffering capacity was increased with high EGTA or BAPTA in the pipette or when the hyperpolarization magnitude was increased by switching holding potentials. These two phenomena are consistent with the features of TRPV6 and readily distinguishable from that of the store-operated cation channel, which is also calcium permeable with high selectivity but activated after intracellular Ca²⁺-store depletion (Putney, 1986; Voets et al., 2001; Bödding et al., 2003). In addition, the current showed calcium autoinhibition and was enhanced in divalent-free solution with a negative slope in the current–voltage relationship, which is also another fingerprint of TRPV6 currents rather than store-operated cation channels

(Schindl et al., 2002; Hoenderop et al., 2005). Our data also showed that the hyperpolarization-activated inactivating current was abolished by removal of extracellular Ca²⁺ under conditions of a low calcium buffering effect (e.g., 0.1 mM EGTA), further supporting the idea that the TRPV6 channel is constitutively open under physiological conditions. Together with other biophysical and pharmacological properties demonstrated in this study, including positive reversal potential, inhibition by extracellular acidosis but enhancement by alkalosis, and blockade by lanthanum, loss of selectivity and a time-dependent increase in divalent-free solution, and strong inward rectifying current–voltage relationship (Vennekens et al., 2001; Peng et al., 2003; Hoenderop et al., 2005), these lines of evidence suggest that the TRPV6
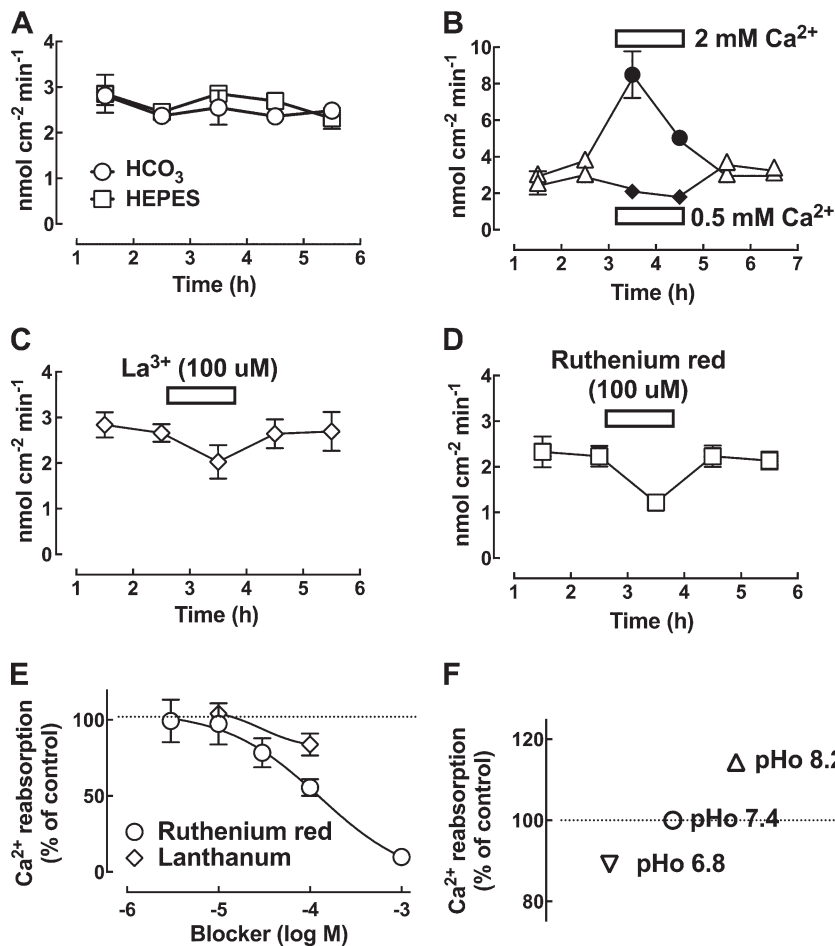
Figure 10. **Ca²⁺-reabsorption function of the perfused rat cauda epididymis.** (A) Ca^{2+} reabsorption by the rat cauda epididymis when perfused with 1 mM Ca^{2+}-containing bicarbonate (HCO_3)- or HEPES-buffered Krebs solution at pH 7.4. (B) The rate of Ca^{2+} reabsorption by the rat corpus epididymis was significantly higher at a higher concentration of luminal Ca^{2+} (2 mM) versus that at a low Ca^{2+} concentration (0.5 mM). (C and D) Time profile showing the reversible inhibition effect of ruthenium red (100 µM) on the rate of Ca^{2+} reabsorption by the rat cauda epididymis. The solution was HEPES-buffered Krebs at pH 7.4. The calculated error bar was within the data point. (E) Dose-dependent inhibition relationship of ruthenium red on Ca^{2+} reabsorption. (F) The rate of Ca^{2+} reabsorption by the rat cauda epididymis was slightly attenuated by changing the perfusing solution from pH 7.4 to 6.8, but it was slightly enhanced when the pH was changed to 8.2. The pH of the solution was buffered with HEPES (n = 5 rats per point). The dotted line indicates the zero current levels. Error bars represent SEM.

channel is present and constitutively active in native principal cells of the rat cauda epididymis.

It has been shown that the epithelial cells lining the epididymal tubule of rats and humans secrete chloride ions when stimulated with agents by involving intracellular cAMP- and Ca^{2+}-dependent Cl^- conductance (Huang et al., 1993). cAMP-activated conductance resembles cystic fibrosis transmembrane regulator conductance, which is well characterized using short-circuit current and patch-clamp techniques in the epididymis and involved in apical chloride secretion of principal cells and secondarily fluid secretion (Huang et al., 1992, 1993; Leung and Wong, 1992; Wong, 1998), whereas the precise role and molecular identity of Ca^{2+}-dependent chloride conductance in epididymal epithelium remains to be established. In this study, we measured a conductance that was activated by depolarizing voltages and mainly contributed to the outward whole-cell currents of principal cells. This conductance was not suppressed by Cs^+-filled pipette solutions but was obviously attenuated by high EGTA-loaded pipette solutions. In addition, it showed time and voltage sensitivity and calcium dependence comparable to the classical CaCC. Moreover, it showed pharmacological sensitivity toward the effective blocker for CaCC, niflumic acid, by which

we excluded the chloride channel accessory protein (CLCA) family as candidates for this conductance because they were not blocked by niflumic acid (Huang et al., 2012a). We therefore speculated that the candidate might be from the bestrophin (BEST) family, which have been proposed as the molecular candidates for CaCC. However, although the biophysical kinetics of BEST1 in human retinal pigment epithelium cells did not match well with the native CaCC, it has been reported to be the volume-regulated chloride channel in spermatozoa (Milenkovic et al., 2015). BEST2 was found in the basolateral membrane of colonic epithelial goblet cells, rather than in the apical membrane of Cl^--secreting enterocytes, and functioned as HCO_3^- channel (Yu et al., 2010). Another potential candidate may be from the TMEM16 family (particularly TMEM16A), because their biophysical kinetics match well with the classical CaCC (Caputo et al., 2008; Schroeder et al., 2008; Yang et al., 2008). From the data-mining study of the Male Reproductive Genetics database, we found that only three TMEM16 isoforms (TMEM16A, TMEM16B, and TMEM16D) have been reported in the rat epididymis. Considering that TMEM16A and TMEM16B, but not TMEM16D, exhibit the same biophysical kinetics as the CaCC (Caputo et al., 2008;

Schroeder et al., 2008; Yang et al., 2008; Huang et al., 2012a), and because TMEM16B mRNA was detected only in the head region (as reported in the Male Reproductive Genetics database) and TMEM16D mRNA was only found in the initial segment and the body region of epididymis (unpublished data), both TMEM16B and TMEM16D are unlikely to be the candidates. We consistently detected TMEM16A mRNA along the efferent duct and epididymis and confirmed its protein colocalized with TRPV6 in the apical membrane of principal cells. All these lines of evidence demonstrated that TMEM16A is constitutively functional as the CaCC and cooperates with TRPV6 in principal cells of the epididymis, although our data could not exclude other candidates for CaCC in these cells.

Cell phenotypes

Our results could have been influenced by the variation in the predominant cell types present in the epithelium of epididymis. Principal cells in intact epididymal epithelium phenotypically have stereocilia on their apical membranes, and after cell isolation, we still observed microvilli structures in a portion of membranes as well as polarized cell contents; however, clear cells might also share similar phenotypes, even though their microvilli are expected to be minimal during the resting state (Shum et al., 2008, 2011). To separate these two cell groups and to obtain a consistent interpretation of the electrophysiological results, we took into account the cell capacitance and input resistance, as indicated in Fig. 2, whole-cell current patterns, and the conductance responses upon designed stimulations. Thus, the cells with slightly larger cell capacitance and higher input resistance, presumably clear cells, which also showed different current patterns and responses than principal cells, were excluded from this study. The other cell types, which did not bear stereocilial structures on their membrane or obvious polarized cellular contents and were very likely the basal cells, showed significantly higher input resistance but smaller cell capacitance (Fig. 2). When we deliberately recorded these cells, their cell capacitance and hence membrane surface area were almost ∼50% smaller than that of microvilli-bearing cells (i.e., principal and clear cells). This is in accord with the observation that these cells looked smaller under the microscope and that the microvilli could increase the surface area. If a specific membrane capacitance of 1 µF•cm^{-2} is assumed, the ∼5 pF found for basal-like cells predicts a membrane surface of 500 µm^2, only half the size of that of principal cells and clear cells. In addition to the passive membrane properties, the current patterns recorded from the basal-like cells were quite consistent but distinct from that of principal cells and clear-like cells, and functional characterization of these currents is worth future investigations. It is worth emphasizing that the data presented in this study were from freshly isolated epithelial cells (i.e., the latest recordings of cells were made the day after cell isolation). We did observe a difference in passive membrane properties and current patterns in cells cultured for several days, and they usually showed a significantly larger cell capacitance and very different current patterns, as reported previously (Cheung et al., 2005).

Implication of the functional coupling of TRPV6 and TMEM16A in the epididymal epithelium

Our present work is consistent with the studies of genetic deletion and mutated mouse models that have demonstrated the essential role of TRPV6 in calcium transport across epithelia and in calcium homeostasis in the epididymis and, eventually, male fertility (Hoenderop et al., 2005; Weissgerber et al., 2011, 2012; Fecher-Trost et al., 2013). TRPV6 is one of the two epithelial Ca^{2+} channels used for transcellular Ca^{2+} absorption in epithelial tissues; the other channel is TRPV5 (Hoenderop et al., 2005; Stoerger and Flockerzi, 2014). TRPV5 is the predominant isoform found in kidney, whereas TRPV6 is found in the intestines, although these tissues coexpressed both isoforms in a region-dependent manner. However, only TRPV6 is expressed in the male excurrent duct, as demonstrated in this study and others (Weissgerber et al., 2011; Oliveira et al., 2012). TRPV5/TRPV6-mediated transcellular Ca^{2+} absorption is a multistep process, which begins with passive Ca^{2+} entry through apical Ca^{2+} channels and is followed by diffusion of Ca^{2+} through the cytosol, facilitated by binding to Ca^{2+}-binding protein (calbindin-D$_{28k}$ in the kidney and epididymis and calbindin-D$_{9K}$ in the intestine) and eventually extrusion of Ca^{2+} across the basolateral membranes by the energy-dependent Na$^+$/Ca^{2+} exchangers and Ca^{2+}-ATPase operating against the Ca^{2+} electrochemical gradient (Hoenderop et al., 2005; Oliveira et al., 2012). From the point of view of energy input, it is suggested that the initial step of passive entry through TRPV5/TRPV6 channels in the apical membranes is the rate-limiting step. It has been reported that TRPV6 activity is supported by intracellular Mg-ATP via lipid kinases and the PIP$_2$ pathway (Zakharian et al., 2011). This suggests that despite no direct evidence that TRPV6 uses ATP as the energy source, it relies on ATP indirectly. In the present study, Mg-ATP at millimolar levels was included in the pipette solutions for electrophysiological experiments. This may explain the discrepancy for the negligible TRPV6 conductance in some native epithelial cells (Stoerger and Flockerzi, 2014), as under those experimental conditions, the intracellular Mg-ATP concentration and/or lipid kinase and PIP$_2$ activities might be insufficient for TRPV6 activity. Nevertheless, although it is now known that TRPV6 is regulated at the level of transcription via the vitamin D signaling axis and intracellular trafficking via BSPY-interacting protein as well as by the extracellular proton

and Ca^{2+} and Mg^{2+} ions (Hoenderop et al., 2005; Schoeber et al., 2007; Stoerger and Flockerzi, 2014), the associated proteins for TRPV6 functional activity at the plasma membrane have not yet been elucidated.

Our results show that CaCC (i.e., TMEM16A) was dependent on the presence of extracellular Ca^{2+} and TRPV6 conductance in epididymal principal cells. It is known that CaCC or TMEM16A channels are highly sensitive to intracellular Ca^{2+}. The resting intracellular Ca^{2+} level ($\sim$100 nM in most cell types; Large and Wang, 1996; Eggermont, 2004; Leblanc et al., 2005) is already the activation threshold level of CaCC or TMEM16A (Romanenko et al., 2010), and the activation EC_{50} is 126 nM for CaCC in native salivary acinar cells, 165 nM in smooth muscle cells, and 196 nM in TMEM16A overexpressed HEK293 cells (Large and Wang, 1996; Romanenko et al., 2010). Consistent with our electrophysiological results for CaCC conductance, TMEM16A channels were found to open at normal levels of cell membrane potential (Romanenko et al., 2010), at which the TRPV6 channels exhibit considerable calcium permeability, as demonstrated in the current–voltage relation in this study and others (Hoenderop et al., 2005). Because increases in intracellular $[Ca^{2+}]$ can be lethal to cells, intracellular $[Ca^{2+}]$ has to be tightly controlled. The spatial distribution of the Ca^{2+} is an important signal, and there are indications that TMEM16A reacts to local Ca^{2+} changes in the proximity space of sub–plasma membrane (Paradiso et al., 2001; Huang et al., 2012a). We therefore hypothesize that Ca^{2+} entry through constitutively open TRPV6 channels causes a local increase in intracellular Ca^{2+} levels and membrane potential depolarization, and CaCC or TMEM16A at the apical membrane of epididymal principal cells is thereby activated to bring the membrane potential back to normal levels. Our patch-clamp and fluorescent membrane potential data are consistent with the notion that both TRPV6 and TMEM16A constitutively contribute to the regulation of resting potential in principal cells and that TMEM16A-mediated conductance is dependent on TRPV6-mediated calcium influx, which in turn regulates the constitutive activity of TRPV6 by electrical coupling. This interplay hypothesis is further supported by the apical colocalization of TRPV6 and TMEM16A in principal cells of the epididymis. A schematic view of our current TRPV6–TMEM16A coupling model for transcellular calcium transport regulation in principal cells is illustrated in Fig. 11.

The physiological functions of TMEM16A have been described in various cell types, including the epithelia of airway and salivary glands, smooth muscle cells, sensory neurons, and interstitial cells of Cajal (Huang et al., 2009, 2012a). TMEM16A genetic disruption in mice leads to lethal defects and severe malformation of tracheal cartilage rings (Rock et al., 2008). In adult exocrine epithelial tissues, the activation of CaCC is known
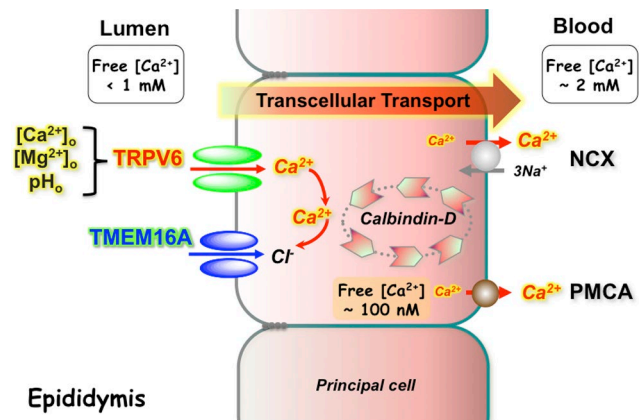

Figure 11. **Schematic representation of a coupling mechanism between TRPV6 and TMEM16A in the homeostatic regulation of calcium in the epididymis.** Both TRPV6 and TMEM16A are expressed in the apical membrane of principal cells. Constitutive activity of TRPV6 is subjected to regulation by extracellular divalent ions (Ca^{2+} and Mg^{2+}) and protons. The influx of extracellular Ca^{2+} ions via TRPV6 primes the activity of TMEM16A at the proximity membranes. The locally raised calcium ions bind with calbindins and are then extruded by the Na^+/Ca^{2+} exchangers (NCX) and ATP-dependent Ca^{2+}-ATPase (PMCA) at the basolateral membrane, as described in the Discussion with references therein.

to be the rate-limiting step for fluid secretion, and TMEM16A has been proposed to be the potential therapeutic target in diseases such as cystic fibrosis, asthma, and cancer (Huang et al., 2012a). More recently, TMEM16A has been reported to mediate mucin secretion in nasal epithelium and plays an important role in upper airway inflammatory diseases (Huang et al., 2012b; Lin et al., 2015; Zhang et al., 2015). The present study demonstrating the functional coupling between TRPV6 and TMEM16A in epididymal epithelial cells implies that TRPV6 channels are not only involved in calcium uptake but also participate in chloride and fluid transportation and probably mucin secretion via calcium influx from the extracellular space and activation of TMEM16A located in the proximity of the apical membrane of principal cells.

It has been reported that the intracellular concentration of chloride was $\sim$62 mM in the rat epididymal cells (Huang et al., 1994). In the present study, the measured resting potential of principal cells has a mean value of 24 mV, ranging from -5.8 to -38.5 mV. This value is comparable with previously reported values of -21 and -30 mV for caput and cauda epididymal epithelial cells, respectively (Cheung et al., 1976). The variation in the measured resting potential is consistent with the notion of an interplay between TRPV6 and TMEM16A. We speculate that the slightly positive potential from the resting potential might be the result of the constitutive activity of TRPV6 and flavors the outward current of chloride and thus chloride influx into the cell when

TMEM16A is open, thereby leading to hyperpolarization and chloride absorption. In cells with slightly negative potential than the resting, both inward currents from TRPV6 and TMEM16A are flavored, which could lead to calcium in and chloride out when TMEM16A is open, in which case the cell depolarizes and secretes chloride. Applying this analogy to the reported luminal chloride ion concentration in the epididymal fluid, which is ~23.6 mM in the rat cauda epididymis (Levine and Marsh, 1971), corresponds with the reversal potential for chloride of about 25 mV. If principal cells hold the same resting membrane potential, constitutively active TRPV6 triggering the opening of TMEM16A would then flavor an inward current and thus chloride secretion from cells into the lumen. Consistently, it has been reported that secretion of chloride occurs at a resting potential that is more negative than the reversal for chloride ions (Frizzell and Hanrahan, 2012).

Although this secretion process is worthy of further investigations, our results show that TRPV6 and TMEM16A participate in calcium homeostasis in the epididymis, which is supported by results from in vivo microperfusion of rat cauda epididymis, in which luminal calcium reabsorption was inhibited by ruthenium red, a widely used but not completely selective inhibitor of TRPV6 and CaCC (Hoenderop et al., 2005; Kim et al., 2011). Microperfusion of rat cauda epididymis under similar conditions has been demonstrated to be active in fluid transportation (Wong and Yeung, 1978; Wong, 1988). In addition, involvement of CaCC in calcium-dependent chloride-driven fluid transportation of rat epididymis has been described (Huang et al., 1992, 1993), and TMEM16A is now known to contribute to chloride secretion in other epithelia (Frizzell and Hanrahan, 2012) and potentially participate in other calcium-dependent secretion processes, such as epididymosome or vesicle secretion, as indicated by TRPV6- and TMEM16A-labeled small vesicles in the luminal contents and on the sperm surface.

The epididymal fluid is maintained at a low calcium acidic pH to keep sperm dormant during maturation and storage in the epididymis (Levine and Marsh, 1971; Carr and Acott, 1984; Hong et al., 1984), and it is intriguing that TRPV6 exhibits the biophysical properties such as autoinhibition by extracellular calcium and alkaline pH–dependent activation. We speculate that Ca^{2+} transport via a TRPV6-mediated process and subsequent fluid transportation via a TMEM16A-dependent pathway are minimally active under resting physiological conditions, in which the pH of luminal cauda epididymal fluid is 6.8 and the calcium level is in the submillimolar range (Levine and Marsh, 1971; Turner, 2002; Da Silva et al., 2007). However, it could become prominent after priming the epithelium with stimuli, such as alkaline pH after bicarbonate secretion, or when extracellular Ca^{2+} and Mg^{2+} ionic concentrations are altered. Although more

studies are required to elucidate the interplay between TRPV6 and TMEM16A, this study is consistent with the notion that homeostatic maintenance of epithelial physiology is intricate but important for epididymal function during sperm maturation and protection.

REFERENCES

Bödding, M., C. Fecher-Trost, and V. Flockerzi. 2003. Store-operated Ca2+ current and TRPV6 channels in lymph node prostate cancer cells. *J. Biol. Chem.* 278:50872–50879. http://dx.doi.org/10.1074/jbc.M308800200

Caputo, A., E. Caci, L. Ferrera, N. Pedemonte, C. Barsanti, E. Sondo, U. Pfeffer, R. Ravazzolo, O. Zegarra-Moran, and L.J. Galietta. 2008. TMEM16A, a membrane protein associated with calcium-dependent chloride channel activity. *Science.* 322:590–594. http://dx.doi.org/10.1126/science.1163518

Carr, D.W., and T.S. Acott. 1984. Inhibition of bovine spermatozoa by caudal epididymal fluid: I. Studies of a sperm motility quiescence factor. *Biol. Reprod.* 30:913–925. http://dx.doi.org/10.1095/biolreprod30.4.913

Cheung, K.H., G.P. Leung, M.C. Leung, W.W. Shum, W.L. Zhou, and P.Y. Wong. 2005. Cell-cell interaction underlies formation of fluid in the male reproductive tract of the rat. *J. Gen. Physiol.* 125:443–454. http://dx.doi.org/10.1085/jgp.200409205

Cheung, Y.M., J.C. Hwang, and P.Y. Wong. 1976. Epithelial membrane potentials of the epididymis in rats [proceedings]. *J. Physiol.* 263:280P.

Chow, B.K., K.H. Cheung, E.M. Tsang, M.C. Leung, S.M. Lee, and P.Y. Wong. 2004. Secretin controls anion secretion in the rat epididymis in an autocrine/paracrine fashion. *Biol. Reprod.* 70:1594–1599. http://dx.doi.org/10.1095/biolreprod.103.024257

Cooper, T.G. 2007. Sperm maturation in the epididymis: a new look at an old problem. *Asian J. Androl.* 9:533–539. http://dx.doi.org/10.1111/j.1745-7262.2007.00285.x

Dacheux, J.L., and F. Dacheux. 2014. New insights into epididymal function in relation to sperm maturation. *Reproduction.* 147:R27–R42. http://dx.doi.org/10.1530/REP-13-0420

Da Silva, N., W.W. Shum, J. El-Annan, T.G. Păunescu, M. McKee, P.J. Smith, D. Brown, and S. Breton. 2007. Relocalization of the V-ATPase B2 subunit to the apical membrane of epididymal clear cells of mice deficient in the B1 subunit. *Am. J. Physiol. Cell Physiol.* 293:C199–C210. http://dx.doi.org/10.1152/ajpcell.00596.2006

Eggermont, J. 2004. Calcium-activated chloride channels: (un)known, (un)loved? *Proc. Am. Thorac. Soc.* 1:22–27. http://dx.doi.org/10.1513/pats.2306010

Fecher-Trost, C., U. Wissenbach, A. Beck, P. Schalkowsky, C. Stoerger, J. Doerr, A. Dembek, M. Simon-Thomas, A. Weber, P. Wollenberg, et al. 2013. The in vivo TRPV6 protein starts at a non-AUG triplet, decoded as methionine, upstream of canonical

180

Ion channel coupling in epithelial ion transport | Gao et al.

initiation at AUG. *J. Biol. Chem.* 288:16629–16644. http://dx.doi .org/10.1074/jbc.M113.469726

Frizzell, R.A., and J.W. Hanrahan. 2012. Physiology of epithelial chloride and fluid secretion. *Cold Spring Harb. Perspect. Med.* 2:a009563. http://dx.doi.org/10.1101/cshperspect.a009563

Hermo, L., and B. Robaire. 2002. Epididymal cell types and their functions. *In* The Epididymis: From Molecular to Clinical Practice. A Comprehensive Survey of the Efferent Ducts, the Epididymis and the Vas Deferens. B. Robaire, and B.T. Hinton, editors. Kluwer Academic, Plenum, New York. 81–102.

Hoenderop, J.G., B. Nilius, and R.J. Bindels. 2005. Calcium absorption across epithelia. *Physiol. Rev.* 85:373–422. http://dx .doi.org/10.1152/physrev.00003.2004

Hong, C.Y., B.N. Chiang, and P. Turner. 1984. Calcium ion is the key regulator of human sperm function. *Lancet.* 2:1449–1451. http:// dx.doi.org/10.1016/S0140-6736(84)91634-9

Hong, C.Y., B.N. Chiang, J. Ku, Y.H. Wei, and J.C. Fong. 1985. Calcium antagonists stimulate sperm motility in ejaculated human semen. *Br. J. Clin. Pharmacol.* 19:45–49. http://dx.doi.org /10.1111/j.1365-2125.1985.tb02611.x

Huang, F., J.R. Rock, B.D. Harfe, T. Cheng, X. Huang, Y.N. Jan, and L.Y. Jan. 2009. Studies on expression and function of the TMEM16A calcium-activated chloride channel. *Proc. Natl. Acad. Sci. USA.* 106:21413–21418. http://dx.doi.org/10.1073/pnas .0911935106

Huang, F., X. Wong, and L.Y. Jan. 2012a. International Union of Basic and Clinical Pharmacology. LXXXV: calcium-activated chloride channels. *Pharmacol. Rev.* 64:1–15. http://dx.doi.org/10 .1124/pr.111.005009

Huang, F., H. Zhang, M. Wu, H. Yang, M. Kudo, C.J. Peters, P.G. Woodruff, O.D. Solberg, M.L. Donne, X. Huang, et al. 2012b. Calcium-activated chloride channel TMEM16A modulates mucin secretion and airway smooth muscle contraction. *Proc. Natl. Acad. Sci. USA.* 109:16354–16359. http://dx.doi.org/10.1073/pnas .1214596109

Huang, S.J., A.Y. Leung, W.O. Fu, Y.W. Chung, T.S. Zhou, P.S. Chan, and P.Y. Wong. 1992. Electrophysiological studies of anion secretion in cultured human epididymal cells. *J. Physiol.* 455:455–469. http://dx.doi.org/10.1113/jphysiol.1992.sp019311

Huang, S.J., W.O. Fu, Y.W. Chung, T.S. Zhou, and P.Y. Wong. 1993. Properties of cAMP-dependent and Ca(2+)-dependent whole cell Cl- conductances in rat epididymal cells. *Am. J. Physiol.* 264:C794–C802.

Huang, S.J., H.C. Chan, and P.Y. Wong. 1994. Adrenaline-regulated Cl- transport in cultured single rat epididymal cells measured by an entrapped Cl-(-)sensitive fluorophore. *J. Physiol.* 474:183–191. http://dx.doi.org/10.1113/jphysiol.1994.sp020012

Jenkins, A.D., C.P. Lechene, and S.S. Howards. 1980. Concentrations of seven elements in the intraluminal fluids of the rat seminiferous tubules, rate testis, and epididymis. *Biol. Reprod.* 23:981–987. http ://dx.doi.org/10.1095/biolreprod23.5.981

Kim, S., L. Ma, and C.R. Yu. 2011. Requirement of calcium-activated chloride channels in the activation of mouse vomeronasal neurons. *Nat. Commun.* 2:365. http://dx.doi.org/10.1038/ ncomms1368

Large, W.A., and Q. Wang. 1996. Characteristics and physiological role of the Ca(2+)-activated Cl- conductance in smooth muscle. *Am. J. Physiol.* 271:C435–C454.

Leblanc, N., J. Ledoux, S. Saleh, A. Sanguinetti, J. Angermann, K. O'Driscoll, F. Britton, B.A. Perrino, and I.A. Greenwood. 2005. Regulation of calcium-activated chloride channels in smooth muscle cells: a complex picture is emerging. *Can. J. Physiol. Pharmacol.* 83:541–556. http://dx.doi.org/10.1139/y05-040

Leung, A.Y., and P.Y. Wong. 1992. Studies of transepithelial Cl- transport in cultured cauda epididymal cells of rats by the short-

circuit current method. *J. Physiol.* 457:391–406. http://dx.doi.org /10.1113/jphysiol.1992.sp019384

Levine, N., and D.J. Marsh. 1971. Micropuncture studies of the electrochemical aspects of fluid and electrolyte transport in individual seminiferous tubules, the epididymis and the vas deferens in rats. *J. Physiol.* 213:557–570. http://dx.doi.org/10 .1113/jphysiol.1971.sp009400

Lin, J., Y. Jiang, L. Li, Y. Liu, H. Tang, and D. Jiang. 2015. TMEM16A mediates the hypersecretion of mucus induced by Interleukin-13. *Exp. Cell Res.* 334:260–269. http://dx.doi.org/10.1016/j.yexcr .2015.02.026

Milenkovic, A., C. Brandl, V.M. Milenkovic, T. Jendryke, L. Sirianant, P. Wanitchakool, S. Zimmermann, C.M. Reiff, F. Horling, H. Schrewe, et al. 2015. Bestrophin 1 is indispensable for volume regulation in human retinal pigment epithelium cells. *Proc. Natl. Acad. Sci. USA.* 112:E2630–E2639. http://dx.doi.org/10.1073/ pnas.1418840112

Oliveira, A.G., D.J. Aquino, G.A. Mahecha, and C.A. Oliveira. 2012. Involvement of the transepithelial calcium transport disruption and the formation of epididymal stones in roosters. *Reproduction.* 143:835–844. http://dx.doi.org/10.1530/REP-12-0034

Paradiso, A.M., C.M. Ribeiro, and R.C. Boucher. 2001. Polarized signaling via purinoceptors in normal and cystic fibrosis airway epithelia. *J. Gen. Physiol.* 117:53–68. http://dx.doi.org/10.1085/ jgp.117.1.53

Peng, J.B., E.M. Brown, and M.A. Hediger. 2003. Epithelial Ca2+ entry channels: transcellular Ca2+ transport and beyond. *J. Physiol.* 551:729–740. http://dx.doi.org/10.1113/jphysiol.2003 .043349

Putney, J.W. Jr. 1986. A model for receptor-regulated calcium entry. *Cell Calcium.* 7:1–12. http://dx.doi.org/10.1016/0143 -4160(86)90026-6

Robaire, B., and B.T. Hinton. 2015. The epididymis. *In* Knobil and Neill's Physiology of Reproduction. T.M. Plant and A.J. Zeleznik, editors. Academic Press, Elsevier Inc. 691–771.

Rock, J.R., C.R. Futtner, and B.D. Harfe. 2008. The transmembrane protein TMEM16A is required for normal development of the murine trachea. *Dev. Biol.* 321:141–149. http://dx.doi.org/10 .1016/j.ydbio.2008.06.009

Romanenko, V.G., M.A. Catalán, D.A. Brown, I. Putzier, H.C. Hartzell, A.D. Marmorstein, M. Gonzalez-Begne, J.R. Rock, B.D. Harfe, and J.E. Melvin. 2010. Tmem16A encodes the Ca2+-activated Cl- channel in mouse submandibular salivary gland acinar cells. *J. Biol. Chem.* 285:12990–13001. http://dx.doi.org /10.1074/jbc.M109.068544

Schindl, R., H. Kahr, I. Graz, K. Groschner, and C. Romanin. 2002. Store depletion-activated CaT1 currents in rat basophilic leukemia mast cells are inhibited by 2-aminoethoxydiphenyl borate. Evidence for a regulatory component that controls activation of both CaT1 and CRAC (Ca(2+) release-activated Ca(2+) channel) channels. *J. Biol. Chem.* 277:26950–26958. http ://dx.doi.org/10.1074/jbc.M203700200

Schoeber, J.P., J.G. Hoenderop, and R.J. Bindels. 2007. Concerted action of associated proteins in the regulation of TRPV5 and TRPV6. *Biochem. Soc. Trans.* 35:115–119. http://dx.doi.org/10 .1042/BST0350115

Schroeder, B.C., T. Cheng, Y.N. Jan, and L.Y. Jan. 2008. Expression cloning of TMEM16A as a calcium-activated chloride channel subunit. *Cell.* 134:1019–1029. http://dx.doi.org/10.1016/j.cell .2008.09.003

Schuh, K., E.J. Cartwright, E. Jankevics, K. Bundschu, J. Liebermann, J.C. Williams, A.L. Armesilla, M. Emerson, D. Oceandy, K.P. Knobeloch, and L. Neyses. 2004. Plasma membrane Ca2+ ATPase 4 is required for sperm motility and male fertility. *J. Biol. Chem.* 279:28220–28226. http://dx.doi.org/10.1074/jbc.M312599200

Shum, W.W., N. Da Silva, M. McKee, P.J. Smith, D. Brown, and S. Breton. 2008. Transepithelial projections from basal cells are luminal sensors in pseudostratified epithelia. *Cell*. 135:1108–1117. http://dx.doi.org/10.1016/j.cell.2008.10.020

Shum, W.W., N. Da Silva, C. Belleannée, M. McKee, D. Brown, and S. Breton. 2011. Regulation of V-ATPase recycling via a RhoA- and ROCKII-dependent pathway in epididymal clear cells. *Am. J. Physiol. Cell Physiol*. 301:C31–C43. http://dx.doi.org/10.1152/ajpcell.00198.2010

Stoerger, C., and V. Flockerzi. 2014. The transient receptor potential cation channel subfamily V member 6 (TRPV6): genetics, biochemical properties, and functions of exceptional calcium channel proteins. *Biochem. Cell Biol*. 92:441–448. http://dx.doi.org/10.1139/bcb-2014-0063

Turner, T.T. 1995. On the epididymis and its role in the development of the fertile ejaculate. *J. Androl*. 16:292–298.

Turner, T.T. 2002. Necessity's potion: inorganic ions and small organic molecules in the epididymial lumen. *In* The Epididymis: From Molecules to Clinical Practice. B.H. B.T. Robaire, editor. Kluwer Academic/Plenum Publishers, New York. 131–150. http://dx.doi.org/10.1007/978-1-4615-0679-9_8

Vennekens, R., J. Prenen, J.G. Hoenderop, R.J. Bindels, G. Droogmans, and B. Nilius. 2001. Modulation of the epithelial Ca2+ channel ECaC by extracellular pH. *Pflugers Arch*. 442:237–242. http://dx.doi.org/10.1007/s004240100517

Voets, T., J. Prenen, A. Fleig, R. Vennekens, H. Watanabe, J.G. Hoenderop, R.J. Bindels, G. Droogmans, R. Penner, and B. Nilius. 2001. CaT1 and the calcium release-activated calcium channel manifest distinct pore properties. *J. Biol. Chem*. 276:47767–47770. http://dx.doi.org/10.1074/jbc.C100607200

Weissgerber, P., U. Kriebs, V. Tsvilovskyy, J. Olausson, O. Kretz, C. Stoerger, R. Vennekens, U. Wissenbach, R. Middendorff, V. Flockerzi, and M. Freichel. 2011. Male fertility depends on Ca²+ absorption by TRPV6 in epididymal epithelia. *Sci. Signal*. 4:ra27. http://dx.doi.org/10.1126/scisignal.2001791

Weissgerber, P., U. Kriebs, V. Tsvilovskyy, J. Olausson, O. Kretz, C. Stoerger, S. Mannebach, U. Wissenbach, R. Vennekens, R. Middendorff, et al. 2012. Excision of Trpv6 gene leads to severe defects in epididymal Ca2+ absorption and male fertility much like single D541A pore mutation. *J. Biol. Chem*. 287:17930–17941. http://dx.doi.org/10.1074/jbc.M111.328286

Wong, P.Y. 1988. Inhibition by chloride channel blockers of anion secretion in cultured epididymal epithelium and intact epididymis of rats. *Br. J. Pharmacol*. 94:155–163. http://dx.doi.org/10.1111/j.1476-5381.1988.tb11510.x

Wong, P.Y. 1998. CFTR gene and male fertility. *Mol. Hum. Reprod*. 4:107–110. http://dx.doi.org/10.1093/molehr/4.2.107

Wong, P.Y., and C.H. Yeung. 1978. Absorptive and secretory functions of the perfused rat cauda epididymidis. *J. Physiol*. 275:13–26. http://dx.doi.org/10.1113/jphysiol.1978.sp012174

Yang, Y.D., H. Cho, J.Y. Koo, M.H. Tak, Y. Cho, W.S. Shim, S.P. Park, J. Lee, B. Lee, B.M. Kim, et al. 2008. TMEM16A confers receptor-activated calcium-dependent chloride conductance. *Nature*. 455:1210–1215. http://dx.doi.org/10.1038/nature07313

Yu, K., R. Lujan, A. Marmorstein, S. Gabriel, and H.C. Hartzell. 2010. Bestrophin-2 mediates bicarbonate transport by goblet cells in mouse colon. *J. Clin. Invest*. 120:1722–1735. http://dx.doi.org/10.1172/JCI41129

Zakharian, E., C. Cao, and T. Rohacs. 2011. Intracellular ATP supports TRPV6 activity via lipid kinases and the generation of PtdIns(4,5)P₂. *FASEB J*. 25:3915–3928. http://dx.doi.org/10.1096/fj.11-184630

Zhang, Y., X. Wang, H. Wang, J. Jiao, Y. Li, E. Fan, L. Zhang, and C. Bachert. 2015. TMEM16A-Mediated Mucin Secretion in IL-13-Induced Nasal Epithelial Cells From Chronic Rhinosinusitis Patients. *Allergy Asthma Immunol. Res*. 7:367–375. http://dx.doi.org/10.4168/aair.2015.7.4.367